HINGELESS FLOW CONTROL OVER AN AIRFOIL VIA DISTRIBUTED ACTUATION

A Thesis

by

ANMOL AGRAWAL

Submitted to the Office of Graduate Studies of
Texas A&M University
in partial fulfillment of the requirements for the degree of

MASTER OF SCIENCE

December 2005

Major Subject: Mechanical Engineering

HINGELESS FLOW CONTROL OVER AN AIRFOIL VIA DISTRIBUTED ACTUATION

A Thesis

by

ANMOL AGRAWAL

Submitted to the Office of Graduate Studies of
Texas A&M University
in partial fulfillment of the requirements for the degree of

MASTER OF SCIENCE

Approved by:

Co-Chairs of Committee,	Othon K. Rediniotis
	J.N. Reddy
Committee Member,	N.K. Anand
Head of Department,	Dennis O'Neal

December 2005

Major Subject: Mechanical Engineering

ABSTRACT

Hingeless Flow Control over an Airfoil via Distributed Actuation. (December 2005)

Anmol Agrawal, B.E., Motilal Nehru National Institute of Technology, India

Co-Chairs of Advisory Committee: Dr. Othon K. Rediniotis
Dr. J.N. Reddy

An experimental investigation was undertaken to test the effectiveness of a novel design for controlling the aerodynamics of an airfoil. A synthetic jet actuator (SJA) was placed inside a NACA 0015 airfoil with its jet at 12.5% of the chord length, hereby referred to as the leading edge actuator. Four centrifugal fans across the span were mounted at 70% of the chord and the jet formed by them was located at 99% of the chord, hereby referred to as the trailing edge actuator. The effects of these actuators on the aerodynamic properties were studied, separately and then in conjunction, with varying angles of attack.

The leading edge actuator delays the onset of stall up to 24 degrees, the maximum angle of attack that could be attained. The control of the aerodynamics was achieved by controlling the amount of separated region. There was no effect of the actuation at lower angles of attack.

The trailing edge actuator provides aerodynamic control at both low and high angles of attack. The study investigated the effect of jet momentum coefficient on the

aerodynamic properties for various angles of attack. The data obtained shows that lift control (in both positive and negative direction) was achieved even at low angles. The actuator enhances the aerodynamic properties by changing the pressure distribution as well as by delaying flow separation.

Study of the combined actuation shows that the synthetic jet actuator was very effective in delaying stall when the trailing edge jet was ejected from the upper surface. For the case when the jet is ejected from the lower surface, there is less control. This can be accounted for by the difference in aerodynamic loading for both cases.

DEDICATION

I dedicate this thesis to my mother and father, Mrs. Asha Agrawal and Mr. Sharad Chandra Agrawal, for their extreme patience and belief in me, without which it would not have been possible to reach this level of education.

ACKNOWLEDGEMENTS

I would like to express my sincere gratitude towards my advisor, Dr. Othon K. Rediniotis, for the immense support and help he has offered throughout this project. His cheerful nature always relieved the tension from me. I learned the fundamentals of aerodynamics and the kind of meticulousness that experimental work requires from him.

I would also like to thank the other members of my advisory committee for their time and patience. Dr. J.N. Reddy introduced me to his current research and its application to fluid dynamics. I really want to express my thanks for his valuable time. Dr. N.K. Anand helped me since my inception at Texas A&M University. As a new graduate student, I found it very comfortable to work with him as a teaching assistant.

Thanks are due to Dr. Lance W. Traub, for things became easy because of his solid concepts of aerodynamics and the experience he has with experiments. Every time I was stuck in implementing something, he had a solution. Anything I know about experimental fluid dynamics, I learned it from my advisor and Dr. Traub.

I would like to thank Rick Allen for his practical suggestions. Thanks to Josh Weimer and Rodney Inmon for the help they offered me for fabricating the model.

Finally, I would like to thank all members of the fluid dynamics lab for their help and encouragement, including Ganesh Mohan for the fruitful discussions of CFD we had and Aaron Kirk for his help with SOLIDWORKS and his car. Thanks to Manoranjan Majji and Bong Su Koh for their understanding and patience with the wind tunnel.

TABLE OF CONTENTS

Page

Page

LIST OF FIGURES

Page

Page

Page

Page

NOMENCLATURE

Nomenclature

α	Angle of attack
CD	Drag coefficient
CL	Lift coefficient
Cm	Pitching moment coefficient
F^+	Strouhal number
$C\mu$	Jet momentum coefficient for leading edge actuator
$C'\mu$	Jet momentum coefficient for trailing edge actuator
f	Frequency
U_∞	Free stream velocity
Re	Reynolds number
δ	Width of trailing edge slot
c	Chord of airfoil
s	Span of airfoil
S_w	Slot width of leading edge actuator
l	Length of slot in spanwise direction
x_{te}	Distance from trailing edge

Abbreviations

LED	Light Emitting Diode

BEC	Battery Eliminator Circuit
SJA	Synthetic Jet Actuator
UAV	Unmanned Aerial Vehicle
IBF	Internally Blown Flap
EBF	Externally Blown Flap
FDM	Fused Deposition Modeling
CAD	Computer Aided Design
DC	Direct Current
PC	Personal Computer
A/D	Analog to Digital
CFD	Computational Fluid Dynamics
RP	Rapid Prototyping

Units

Amp	Ampere
1’	feet
1"	inch
m	meter
m/s	meter per second
Pa	Pascal
rpm	revolution per minute
V	Volts
W	Watt
kg	kilogram

INTRODUCTION

General

Air force is a major unit in any modern war. The era of modern military aircraft has been marked by development of low observable stealth fighters and Unmanned Aerial Vehicles (UAV), which can fool enemy detection systems. Surface of these vehicles is designed to deflect the radar signals away from the receiver. Since the shape of these aircrafts is dictated by stealth considerations with little input from aerodynamics, it becomes crucial to control the flow using virtual shaping methods to attain desirable aerodynamic characteristics. Another need for stealth aircrafts is the absence of hinged components (moving control surface) on the surface of the wings. Actuation of such components can cause the shape of aircraft surface to change, foiling any effort that would have been made towards designing low detection surfaces.

Separation Control

Flow separation is one of the most important issues that need to be addressed. As the angle of attack increases, there is a strong adverse pressure gradient on the suction side of the airfoil. Various mechanisms such as blowing compressed air and suction using external hardware were explored in the beginning of the twentieth century. Flow control methodologies can be classified as active or passive methods. Passive devices do not require any energy to be introduced. Passive devices that have been used for flow

---

This thesis follows the style and format of the *AIAA Journal.*

control include vortex generators (Klausmeyer et al., 1996)[1], distributed roughness, acoustic cavities (Chang et al., 1992)[2], and self excited rods (Huang and Mao, 2002)[3]. Vortex generators enhance the mixing of the fluid in the shear layer. This mixing increases the amount of turbulence in the boundary layer and adds the energy needed to overcome the adverse pressure gradient. Other passive methods mentioned above function by natural tendencies inherent in the fluidic motion. These methods function by creating vortical structures in the flowfield by taking advantage of the harmonic receptivity of the flowfield. The vortical structures influence the mixing of fluid from the free stream velocity into the slower and lower energy boundary layer.

Suction from the surface of an airfoil has been used to remove low energy fluid directly from the boundary layer. This work was begun by Prandtl in 1904 and has been investigated successfully many times since (Kruger, 1947)[4]. Along with suction of the boundary layer, introducing momentum via blowing has been used to energize the low energy region. High pressure air taken from an engine compressor has been used as the source for this momentum. Goodmanson and Gratzer[5, 6] have shown in previous studies how these devices have been used. A jet has been used to blow normal to the flow and enhance the mixing layer (Tillman and Hwang[7] and Gad-el-Hak[8]). The jet can be blown tangentially along a curved surface to take advantage of a phenomenon known as the "Coanda Effect". The tangential jet will contain a pressure gradient normal to the airfoil surface which helps to overcome the adverse pressure gradient of a stalled flow. The pressure gradients that hold the emanating jet to a surface can also be exploited to obtain

an increase in circulation. This is highly desirable as the lift is proportional to the amount of circulation around a body. Recently, the synthetic jet actuator has been studied quite extensively in the areas of enhancement of mixing flows, separation control, wing shaping, and fluidic thrust vectoring. Most existing synthetic jet actuators utilized a small scale low-energy actuation to create micro disturbances into highly receptive regions of a flowfield. The disturbances into these regions create changes in the evolution of the fluid flow. Streamwise vortical structures are created from the small disturbances and energize the boundary layer. Seifert and Pack[9] have demonstrated that in order to gain the desired results from a synthetic jet actuator, there must be one to four vortices produced over the airfoil surface at any given time. Seifert has also shown that the most efficient excitation corresponds to the SJA being oscillated at an optimal non-dimensional frequency. The optimal non dimensional frequency is about one and is derived from the Strouhal number. The non-dimensional frequency is defined to be:

$$F^{+} = f\frac{x_{te}}{U_{\infty}} \tag{1}$$

where, f is the actuator frequency, x_{te} is the distance from the actuator to the trailing edge of the airfoil and U_{∞} is the value of the freestream velocity. Moreover, the literature indicates that jet momentum coefficients (Cμ) of at least 0.002 are necessary before any substantial effects on the flow can be observed. This coefficient is defined as the ratio between the momentum of the jet emanating from the actuator and the

momentum of the freestream. It may be calculated either using the maximum velocity at the slot exit or by using the RMS value of the jet exit velocity. For the results presented here, the jet momentum coefficient was calculated using the maximum value of the velocity of the flow exiting the jet. The expression that defines the coefficient is then (Seifert et al., 1993)[10]:

$$C_{\mu} = \frac{(\rho h u^2)_{jet}}{(\rho C U^2)_{\infty}} \tag{2}$$

where, ρ is the fluid density, h is the width of the jet exit, u is the amplitude of the velocity at the jet exit, C is the reference or characteristic length (for example, in this case the chord length of the airfoil) and the subscript "∞" indicates "freestream". Many of the synthetic jet actuators used in preexisting technical literature have relied on systems that are driven piezoelectrically (Rathnasingham and Breuer[11] and Seifert et al.[12]) or by external hardware (Seifert and Pack[13], McCormick[14] and Greenblatt Wygnanski[15]). This external hardware required for acoustic or pneumatic systems rest mainly outside of the test section of the wind tunnel. Applications typically require that the synthetic jets be small and compact so as to fit inside the control surface of the aircraft the performance of which they were attempting to modify. Although piezoelectric actuators have been light and compact they display poor performance characteristics away from actuator resonance frequencies and the maximum available amplitude is limited. The need for large amplitude was driven by the need to perform at

higher Reynolds or Mach numbers. In previous research by Gilarranz and Rediniotis[16], a compact, high-power synthetic jet actuator was developed to meet the demands for size, weight, efficiency and power density needed for full-scale flow control applications. The creation and more in-depth description of the synthetic jet actuator can be found in Gilarranz et al.[16, 17]. This actuator was advantageous over piezo type actuators due to: its ability to achieve oscillation amplitudes of at least an order of magnitude higher, decoupling of oscillation amplitude and frequency, greater power density, smaller driving voltages, off the shelf construction materials. The use of a synthetic jet actuator to reattach a separated flow field is shown in figures 1 and 2. In figure 1 it can clearly be seen that without actuation the smoke traveled off the surface of the airfoil. With a leading edge actuator (figure 2) in use the smoke conformed to the surface and the separated region was eliminated.

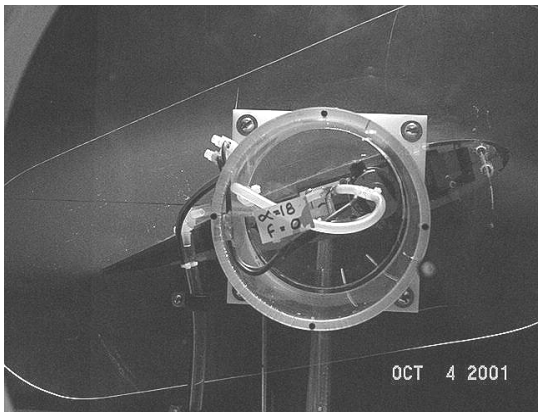

Figure 1: Smoke flow visualization of NACA 0015 airfoil in a flow field at 20 α=20 degrees (Gilarranz et al.[17]). Without actuation.

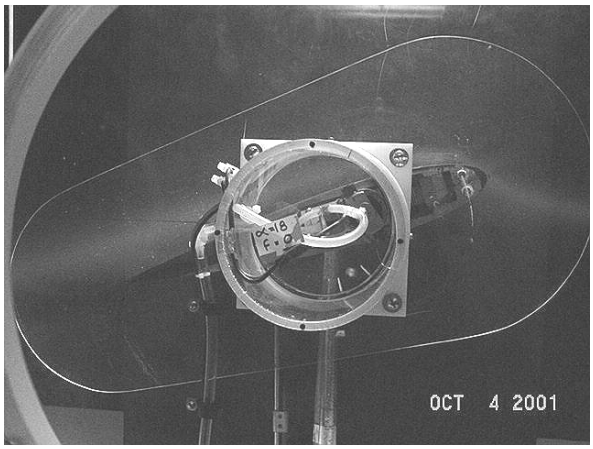

Figure 2: Smoke flow visualization of NACA 0015 airfoil in a flow field at 20 α=20 degrees. (Gilarranz et al.[17]). With actuation.

Jet Flaps

Jet flaps (Davidson 1956)[18] has been a very promising technology in attaining high lift in aircrafts. The idea is demonstrated in figure 3 (b) & (c) together with a typical pressure distribution. The term jet flap implies that a jet is directed to leave the wing trailing edge as a plane jet at an angle to the mainstream, so that an asymmetrical flow pattern and circulation is generated about the airfoil in a manner somewhat analogous to a trailing edge flap. This causes asymmetrical pressure distribution resulting in increase of lift coefficient. The Kutta condition is violated at the trailing edge increasing loading at the trailing part of airfoil, which results in lift enhancement.

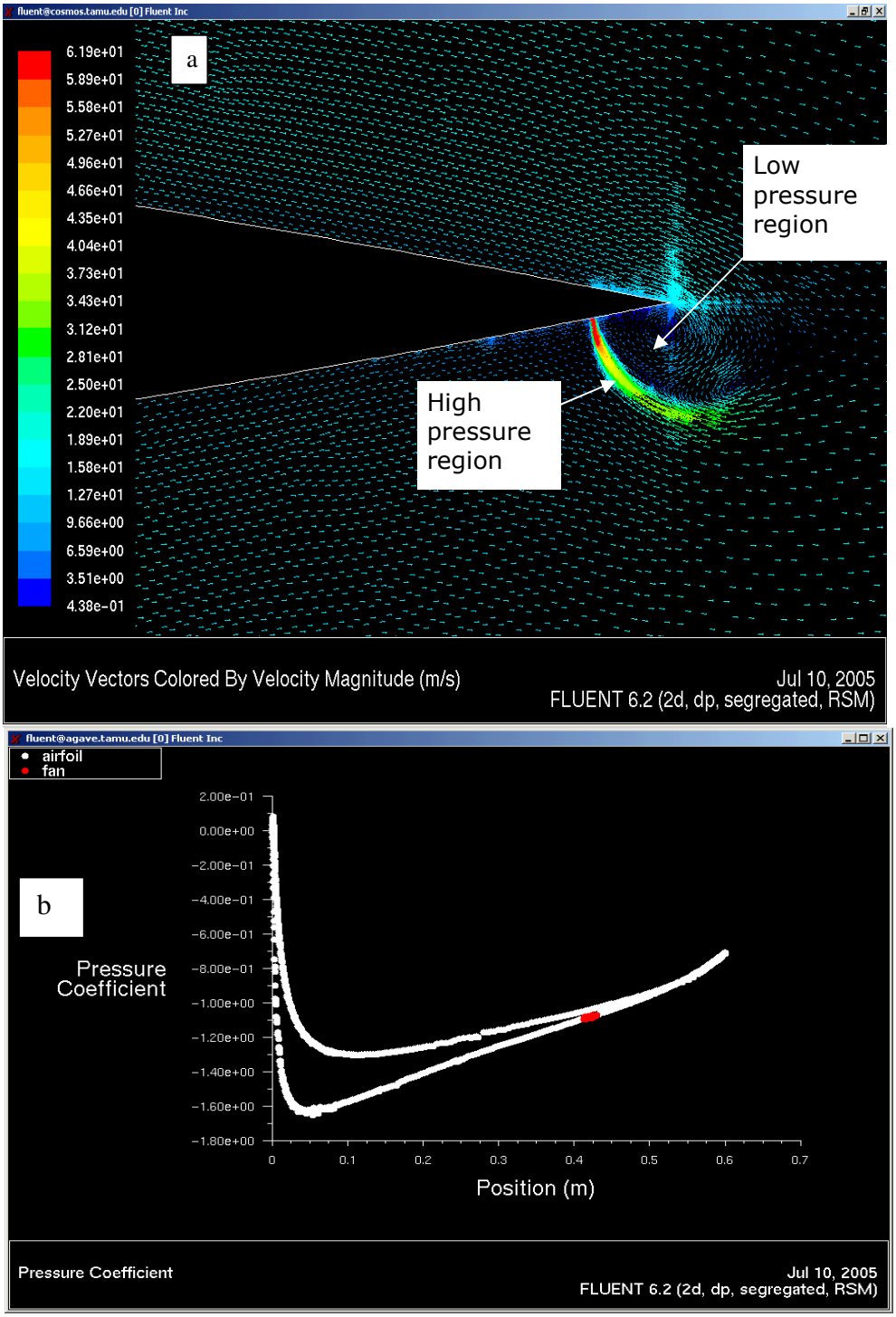

Figure 3: FLUENT simulation of the jet flap effect on an NACA airfoil at $\alpha=2^{o}$. a) Velocity vectors near the jet. b) Pressure distribution on the airfoil with no jet flap.

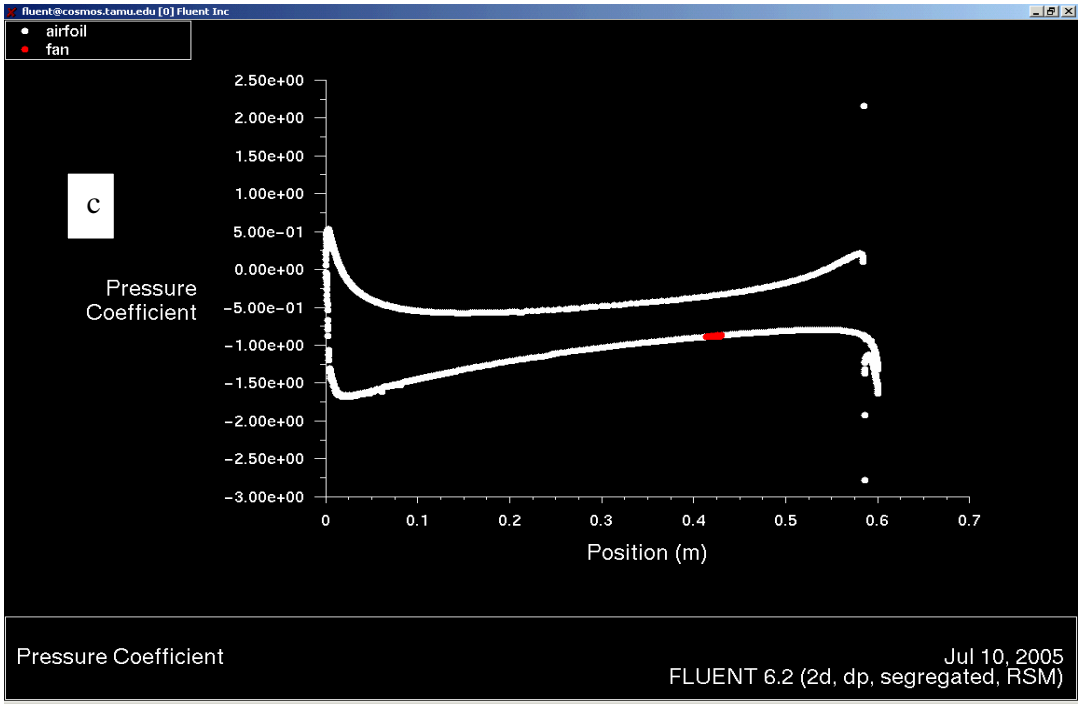

Figure 3: continued. c) Pressure distribution on the airfoil with jet flap.

Various designs that have been proposed (Williams et al.)[19] use engine air bled from the compressor. To facilitate variation of jet angle to the mainstream direction, air is usually ejected from a slot forward of the trailing edge, over a small flap whose angle can be varied as shown in figure 4. Such basic jet flap schemes essentially require the gas to be ducted through the wing and are commonly referred to as "internally blown flap" as shown in figure 4 a. Another such design known as "externally blown flap" (figure 4 b) deploys gas ducts and nozzles outside the wing. In this arrangement, each round jet from the exhaust of jet engines is directed towards the gap of a slotted flap which guides the air over the flap in the form of a flattened jet sheet.

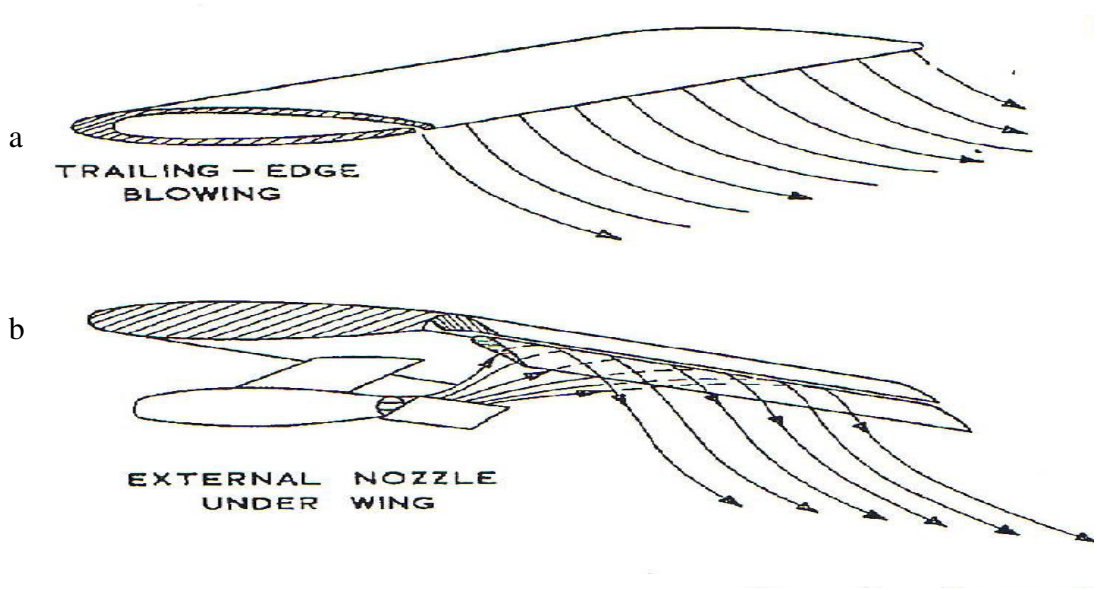

Figure 4: Some jet flap schemes (Williams et al.[19]) a) Internally blowing flap b) Externally blowing flap.

Both of these methods use the air bled from the engine compressor which couples engine performance with jet flaps. The externally blown flap design, even with fixed flap, may not be useful for stealth aircraft, where engines are normally housed inside the wing. The internally blown flap design uses complicated internal tubing whose design is itself a problem. In case of an asymmetric engine failure or misfiring during flight, the results can be catastrophic due to unbalanced roll moments that may be generated.

Trailing Edge Actuator

In the present study, we propose a new design, completely decoupling engines with jet flap and using the advantages of boundary layer suction, whose effects have been explored by Prandtl in early twentieth century.

It is a well known fact that flow separation is a major problem for attaining high lift. The phenomenon occurs at the suction side of the airfoil, when low momentum air in the vicinity of the airfoil surface re-circulates under the influence of adverse pressure gradient. We use centrifugal fans at 70% of the chord length to suck in low energy boundary layer, which is prone to separation. The air sucked is energized and forced out in the form of jet flap perpendicular to the chord. We do not intend to recover jet momentum in the form of propulsive thrust, as the momentum coefficient is too low to detect any force, therefore we eject the jet at an angle of 90 degree with respect to the chord. A symmetrical duct system as shown in figure 5 can be used to eject the jet from the upper, as well as, from the lower surface. The direction of airflow can be regulated by an internal flap mechanism. The objectives of the design are as follows:

1) Increase lift coefficient at low angles of attack.
2) Delay angle of stall, increasing maximum lift coefficient.
3) Create negative lift coefficient in a hingeless fashion, to be able to control roll moment in an aircraft.

This design is completely hingeless and self contained inside the wing. Only wires communicate to the batteries for power supply. Limitations of the leading edge actuator

have been addressed by incorporation of the trailing edge actuator combining the attractive features of boundary layer suction and jet flap technologies. This thesis presents our latest advancement in the development and testing of these flow control technologies.

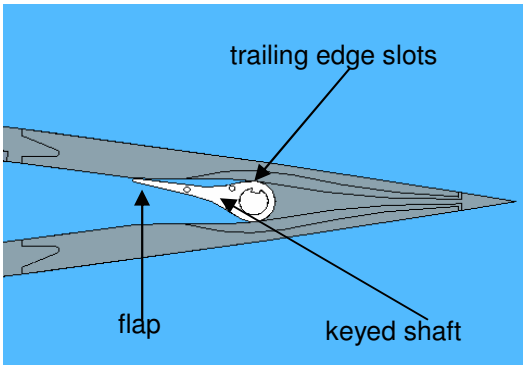

Figure 5: Bidirectional ducting and internal flap mechanism.

DETAILS OF THE WING SURFACE AND LEADING EDGE ACTUATOR DESIGN

General

This section discusses the details of the wing surface and leading edge actuator design. It describes the construction of SJA, plenum and leading edge slots.

Wing Surface

The test wing profile for the tests of the leading and trailing edge actuator is a NACA 0015 airfoil. This shape was chosen due to the ease with which the wing could be manufactured and the available interior space for accommodating the synthetic jet actuator (SJA). The wing has a chord length of 0.60 meters and a span of 0.32 meters. The exterior structure of the wing is comprised of four separate pieces: the front and mid section, the trailing edge section and a section between the trailing edge section and the mid section with holes to match the fans of the trailing edge actuator. The mid section is designed to hold the base plate fitted with an array of fans and motors. Figure 6 shows the details.

Description of Leading Edge Actuator

The leading edge actuator consists of the synthetic jet actuator connected to the skin of the wing through a plenum at 12.5 % of the chord length. The principle of our SJA

driving mechanism is well-developed, and has been extensively utilized in a variety of engines. It consists of a DC motor with its shaft connected eccentrically to a crank, which is in turn connected to the pistons of the SJA (figure 7 a). Due to eccentricity, the

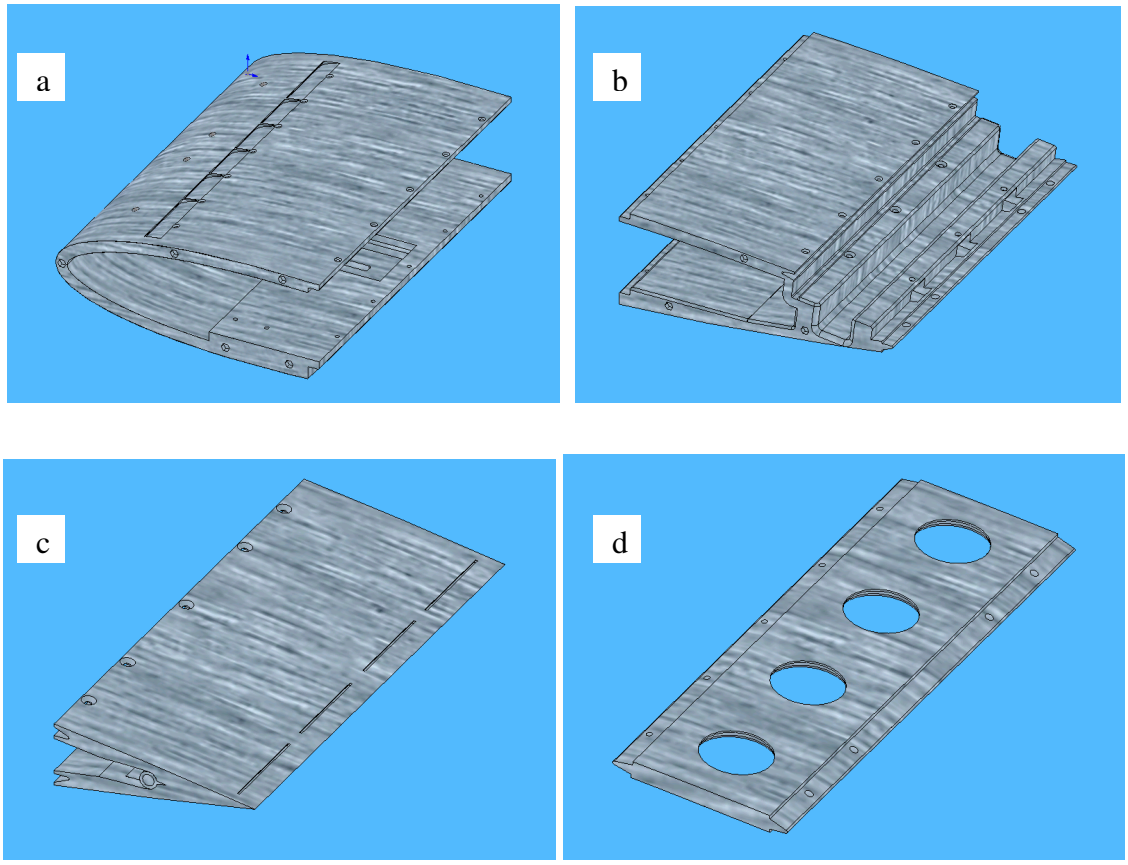

Figure 6: a) Front part of airfoil, made with leading edge slots b) mid section showing recess for fixing fans c) Trailing edge section, showing jet flap slots d) The section used to cover fans.

rotary motion of the motor is translated to linear motion of the SJA pistons. This design offers benefits over, for example, piezoceramic driving mechanisms, since: it can achieve piston oscillation amplitudes at least an order of magnitude higher; it eliminates

the dependence of oscillation amplitude on the oscillation frequency, which plagues piezoceramic mechanisms; with available state-of-the-art, high power-density electric motors it can match and exceed the power densities of piezoceramic mechanisms; it requires significantly smaller driving voltages.

For the present SJA, as shown in figure 7, electric motors drive a series of "off the shelf" small gasoline engines which are used as reciprocating compressors. The cylinder head of each of these engines is perforated and attached to a plenum, which is closed on all sides except for a slot machined on one of the walls. The change in the cavity volume of the plenum causes the pressure inside the cavity to fluctuate, creating the synthetic jet. The use of the available engine technology reduces the effort to manufacture pistons with no leakage, thus simplifying the design and construction of the SJA. As shown in figures 7 a and 7 b, the present SJA array is composed of 6 reciprocating compressors (pistons), which are driven by two DC motors. Each piston has a diameter of 27.7 mm and a peak-to-peak piston stroke of 22 mm. Each DC motor measured 69.8 mm in length and 41.1 mm in diameter, had a maximum power of 800 W and weighed 0.34 kg. The exit slot of the plenum is curved in order to permit the jet to exit tangentially to the surface of the wing, taking advantage of the Coanda effect. Figure 7 c shows a picture of the SJA array illustrating details on cylinder arrangement, slot geometry and cylinder phasing. It should be noted that the cylinders had to be properly phased in order to reduce array vibration. This phasing in turn required the compartmentalization of the plenum, as it is obvious that if the plenum was not divided into six individual

compartments, each one corresponding to each of the six cylinders, the engine phasing would result in zero net volume change in the plenum during an operation cycle and thus no synthetic jet effect. More details on the design and fabrication of the actuator can be found in Gilarranz (2001) and Gilarranz and Rediniotis (2002).

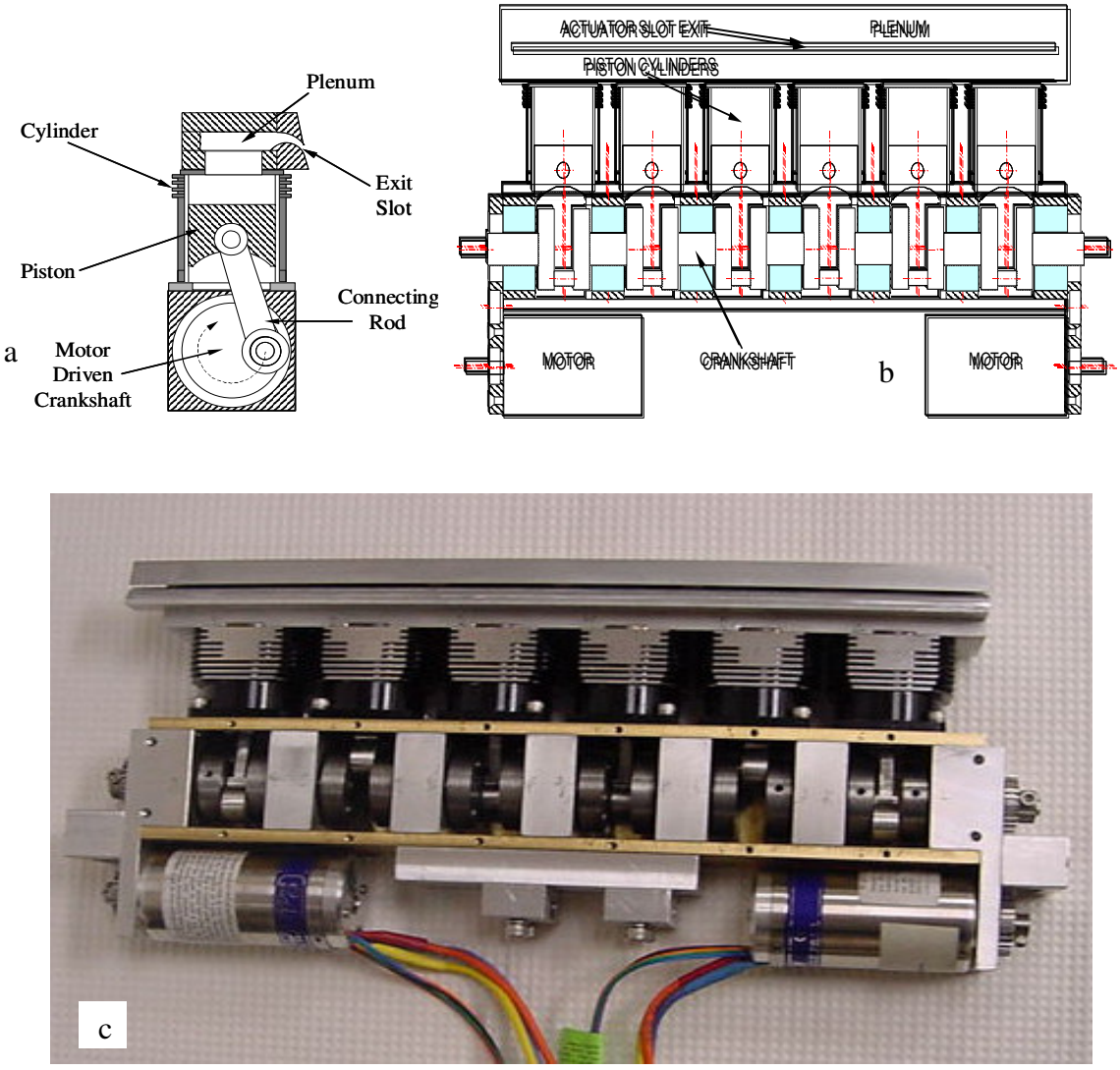

Figure 7: The leading-edge synthetic jet actuator: (a) schematic of single piston and its interface with the plenum, (b) schematic of synthetic jet array, (c) picture of SJA array, showing motor mounting, cylinder phasing, and exit slot geometry with fixed exit area.

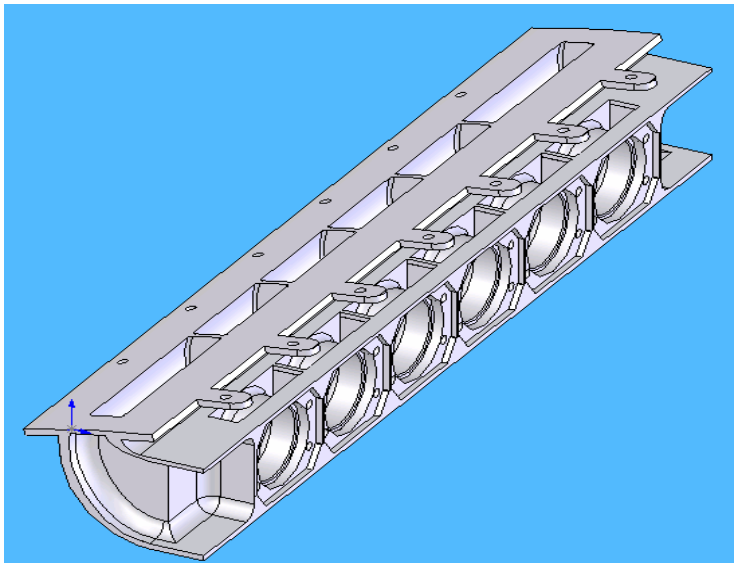

Figure 8: Details of plenum design. It fits into SJA at one end at to front of skin at other.

The plenum shown in figure 8, was designed to serve as an interface to connect the cylinders of the SJA to the leading edge slots made in the surface. The CAD model was used to Rapid Prototype it in our FDM 3000 STRASYS machine using ABS plastic. The leading edge slots were designed such that the mean direction at which air is ejected, makes a low angle (17^o) with the surface of the airfoil. As shown in figure 7 a, there are 6 slots to match 6 cylinders in the SJA. The dimensions of the inner 4 slots are 1.85 x 41 mm^2. The outer slots at each end measure 1.85 x 63mm^2. The outer slots are wider to ensure that effect of the SJA over the entire span of the wing. This assembly of plenum and SJA is connected to the wing as shown in figure 9. Silicon sealant is used at the interface to eliminate any leaks that may occur.

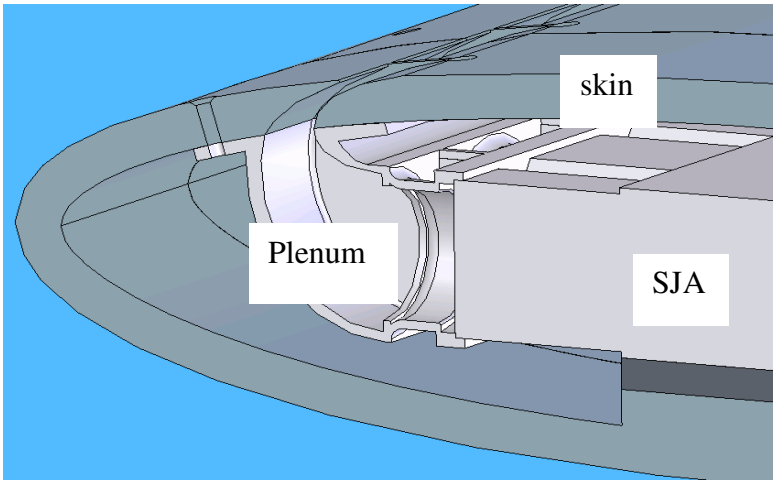

Figure 9: Sectional view of SJA, plenum and skin assembly.

To avoid distortion of the wing due to the weight of SJA, the base is designed to transfer the entire weight of the SJA to the L shaped steel bracket, as shown in figure 10, which pivots the wing on the pyramidical balance.

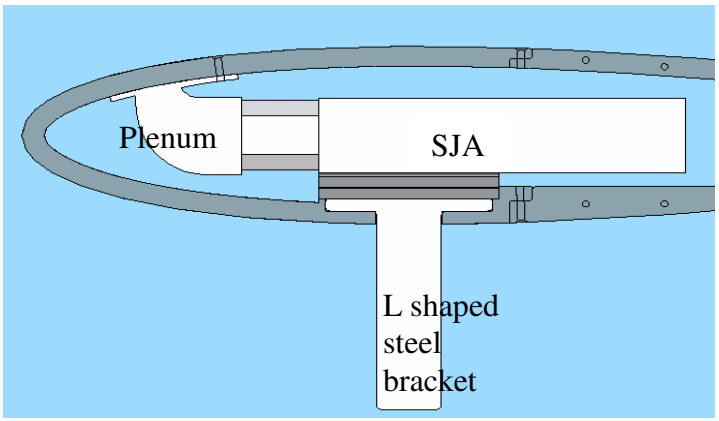

Figure 10: SJA, plenum and wing supported by the L shaped steel bracket (L part not shown here).

TRAILING EDGE ACTUATOR

General

This section discusses details about the design and fabrication of the trailing edge actuator. It talks about the array of fans, the ducting and internal flap mechanism for the construction of the actuator.

Design and Fabrication

The trailing edge actuator consists of two mechanisms - a mechanism to suck the low energy boundary layer inside the airfoil, thus bringing higher momentum air close to the airfoil wall which is less prone to separation, and a mechanism to enhance the aerodynamic loading at the rear of airfoil. For suction of low energy air we use an array of four centrifugal fans at around 70% of the chord length. The fans used here are from Black and Decker. They have an eye diameter of 39 mm and an outer diameter of 68 mm. Each fan consists of 10 blades which are shrouded. Each fan is coupled to an electric motor. These are brushless DC motors capable of running at speed of 20,000 rpm. Each of these motor fan systems is mounted on a thin aluminum plate which is fastened to a recess in the skin, visible in figure 11. The figure also shows the holes made in the skin to match the eye of each fan. The trailing edge actuator is separated from the rest of the airfoil by a wall made while fabricating the skin of the airfoil.

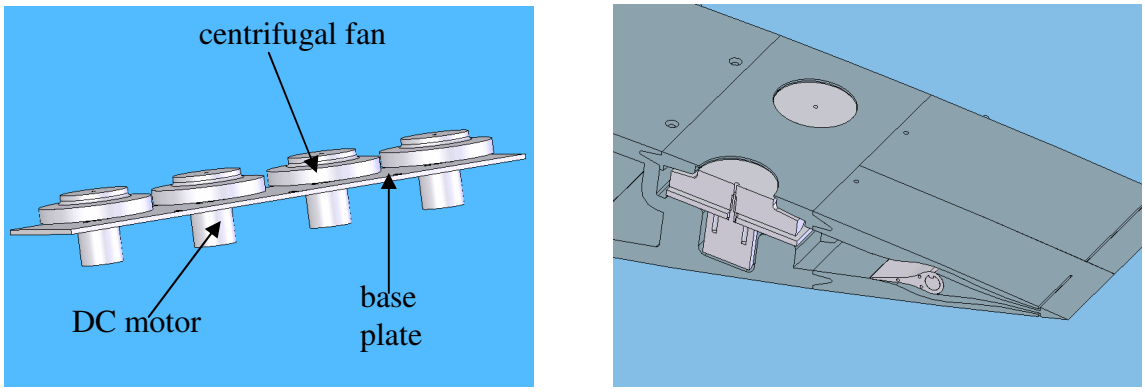

Figure 11: (a) Array of fans mounted on aluminum plate (b) Sectional view showing details of trailing edge actuator.

The cavity formed at the trailing edge ultimately separates in two ducts which communicate to the trailing edge slots as shown in figure 12. An internal flap mechanism controls the direction of the airflow. The flap can be rotated by an aluminum shaft, having a keyhole running through its length, which fits on the key made in the flap.

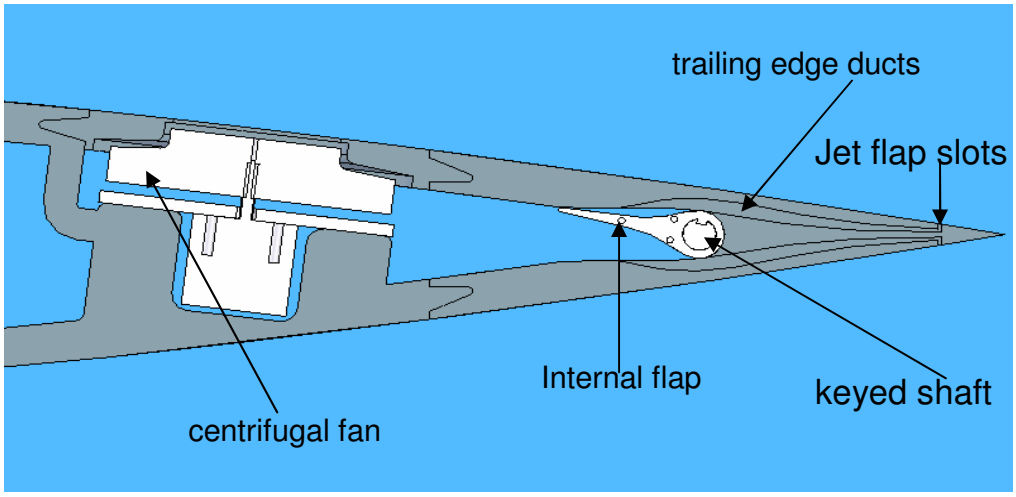

Figure 12: Side view of the airfoil showing details of trailing edge actuator.

The design enables the operation in two modes depending on the position of internal flap as can be observed in figure 13. The first configuration forms a lower jet flap, with the jets ejecting from the lower surface. We also incorporate the ability to eject the jets from the upper surface and investigate their effects on the flowfield in the next section.

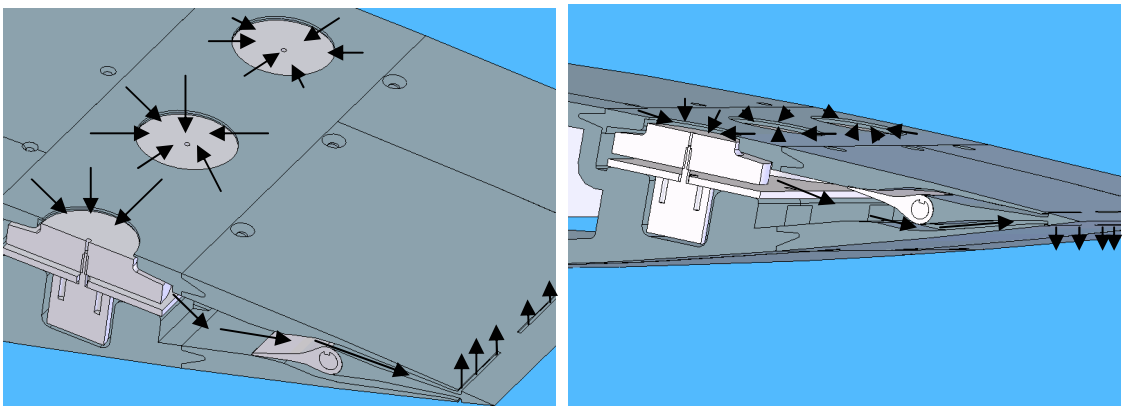

Figure 13: Schematic of airflow around the trailing edge actuator with (a) Jet ejecting from upper surface (b) Jet ejecting from lower surface.

The skin with slots and cavity and internal flap is manufactured by rapid prototyping.

INSTRUMENTATION, FACILITIES, EXPERIMENTAL SETUP AND PROCEDURES

General

Details of instrumentation, setup, facilities and procedures of the test are described in this section.

Instrumentation

The DC motors used in the synthetic jet actuator were controlled by an astro flight electronic motor controller with BEC. Due to overheating of the controller, compressed air was continuously blown over its surface for its safe operation. The motors used for running the fans have an inbuilt chip to control its speed. These motors are powered in parallel using 12 V batteries. Maximum current rating for each motor is 7.5 A. We use a fuse in the power circuit to prevent any overheating that may damage the motor windings. Control wires for all four motors are connected in parallel to the receiver of an FM radio receiver-transmitter control unit. Transmitter throttle shown in the figure on page 23 is adjusted to control the speed of the motors.

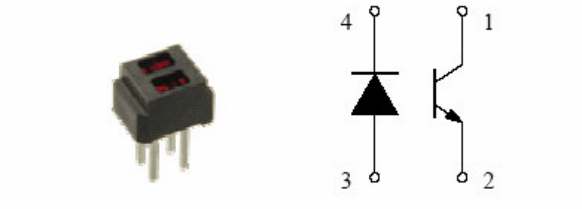

Figure 14: Optoelectronic reflective speed sensor.

Optoelectronic speed sensors shown in figure 14 have been used to measure the frequency of all motors. Each sensor consists of a combination of light emitting diode and photodiode. A reflective aluminum tape is pasted at the bottom of each fan. When a fan runs, in each cycle, as the reflective tape comes over the sensor, light emitted by the LED gets reflected from the tape and goes back to the photodiode causing current to pass through it. This generates a pulsed voltage output, with the frequency of the voltage pulsation being equal to the frequency of the motor. Adequate care has been taken to adjust the length of tape so that we may not register any higher order harmonics due to the response time of each electrical unit in the sensor. The sensors require 5 V input supply, which is supplied from LM 7805 chips. These chips have been powered using standard 12 V batteries. Pulsed voltage output is registered using a multimeters. Figure 15 shows electronic breadboards built to power the sensors used.

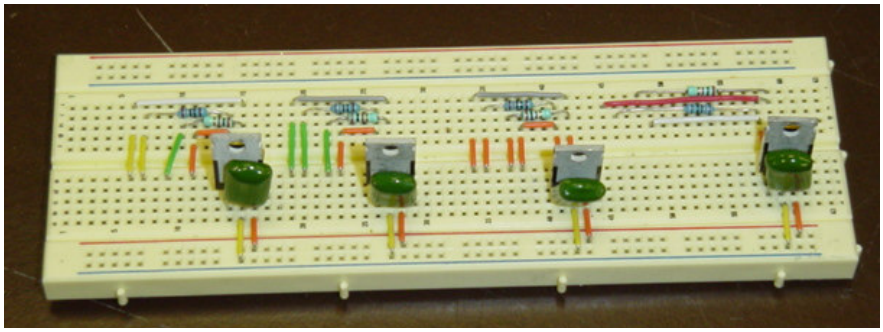

Figure 15: Breadboard showing LM 7805 chips, with capacitors and resistors to build sensor power supply.

Facilities

The aerodynamic tests were performed in the Texas A&M University's 3' x 4' continuous wind tunnel at a freestream velocity (U_∞) of 18 m/s, with a resulting Reynolds number based on the wing chord of Re = 7.1 x 10^5. Unless mentioned otherwise, the results presented correspond to the above-mentioned values. The wind tunnel has a turbulence intensity of 0.5% at a freestream velocity of 18 m/s. The freestream velocity was determined using a wall mounted Pitot tube, manufactured by United Sensors, with a tip diameter of 3.175 mm. Differential pressure was measured using an Omega PX139 series pressure transducer with a range of ±2.0 kPa, which can resolve pressures down to 1Pa. Output of the thermocouple was measured by an Omega I-Series temperature and process monitor with a voltage measurement resolution of 1μvolt.

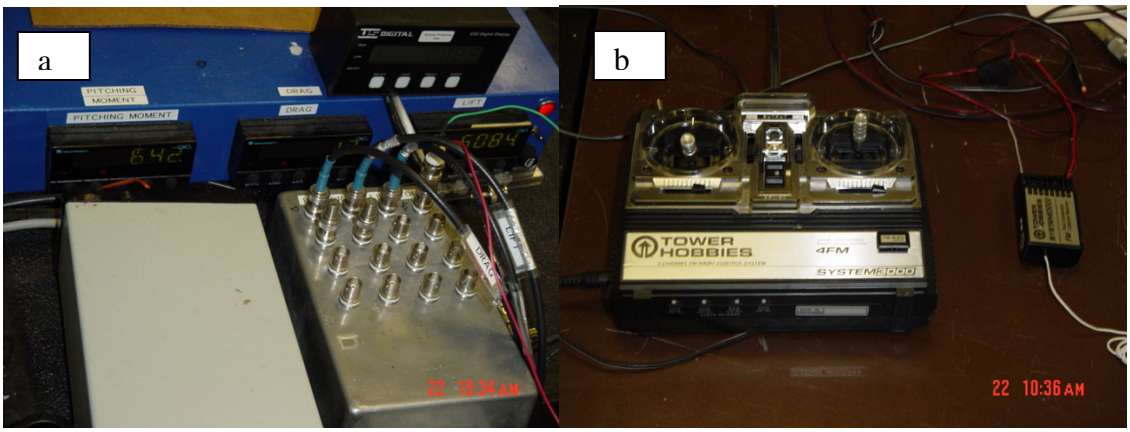

Figure 16: a) 16 bit A/D board and load cells b) Transmitter and receiver system to control motors.

A three component Aerolab pyramidal balance was used for force and moment determination. The balance measures two forces (lift and drag) as well as pitching moment. These components are measured directly by three strain gage load-cells. The accuracy of the balance was estimated at 0.5% of full scale for lift, drag and pitching moment. Through repeated data runs, repeatability of the balance for lift, drag and pitching moment was estimated to be $\Delta CL = 0.005$, $\Delta CD = 0.005$ and $\Delta Cm = 0.003$.

Model pitch (angle of attack) was adjusted using a stepper motor, which was connected to a worm-gear mechanism. A high-resolution optical encoder was connected to the mechanism and its output was fed into the data acquisition program via a digital read out display with a RS232 output. Model angle of attack could be set to within 0.05 deg. Force balance data as well as wind tunnel dynamic pressure and temperature were acquired using a P.C. equipped with a 16 bit A/D board shown in figure 16.

Setup

The sensors are mounted on the base plate as shown in figure 17. Side plates made of Plexiglass are mounted on the sides to – make the flow two dimensional, eliminating any downwash effects and to seal the cavity at the trailing edge so that air sucked in through fans does not escape from the sides. Adhesive caulk is applied at the interface of wing and side plates to ensure proper sealing. Thus the side plates ride with the wing. The model is painted white to remove surface irregularities that resulted from the

manufacturing processes and to help improve flow visualization. The system is then pivoted on the balance strut using the L-shape bracket that emanates from the model and the arm of the bracket is fixed to the pitching strut as shown in figure 18 a. This strut is capable of moving and provides motion for changing the angle of attack of the wing.

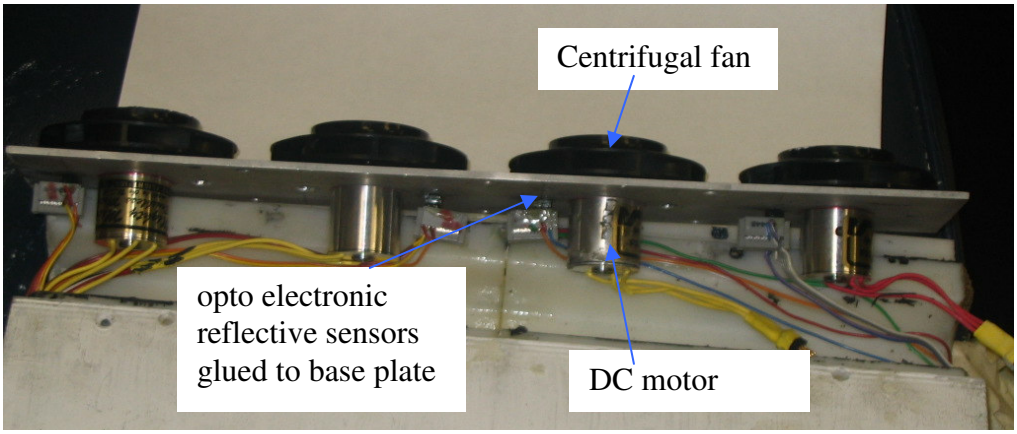

Figure 17: Aluminum base plate showing array of fans, motors and optoelectronic sensors.

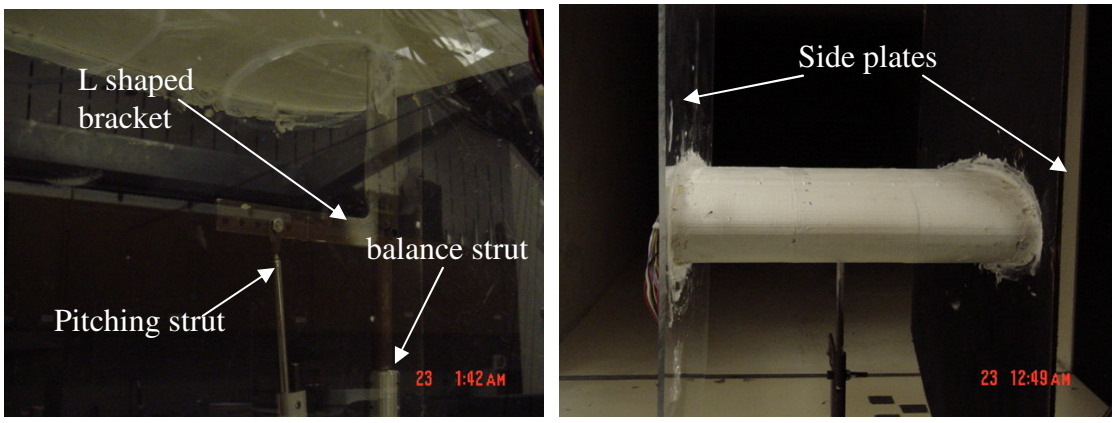

Figure 18: Photographs of the wing mounted in the wind tunnel. a) Balance strut, L-shape bracket and pitching strut b) Wing with side plates.

Actuator Surveys

The process of quantification of the actuator flow field is basically a calibration process. In this section we discuss the method of quantifying the strength of the leading and trailing edge actuators based on actuator frequency.

Characterization of Synthetic Jets

The behavior of the actuator was evaluated by characterizing the flowfield of the actuator. These tests involved the measurement of the instantaneous slot exit velocity of the actuator as a function of frequency. These tests were performed with no airflow inside the tunnel. For the results reported, a hot-wire anemometer was used to measure instantaneous jet velocity at the exit of the SJA slots. The data from the measurement probes were acquired using a P.C. equipped with a 16 bit A/D board. The acquired data included the voltage output of the hot-wire sensor as well as the voltage signal from an optoelectronic sensor, which was used to measure the frequency of operation of the actuator and provide accurate phase referencing information. The hot-wire system consisted of a TSI 1201 hot-wire probe interfaced with an A.A. Lab Systems Anemometer. The system was used in a constant temperature mode.

Characterization of Trailing Edge Actuator

The trailing edge actuator was typified without any airflow past the wing by measuring velocity versus fan frequency. Frequency of each fan was measured against the air velocity at the exit of the corresponding slot. Air velocity was measured using a Pitot tube from United Sensors with a tip diameter of 0.025". Dynamic pressure was read using a Transcat calibrated manometer. Motor frequency was measured using optoelectronic reflective sensors fitted to the aluminum base plate as described earlier.

The measurement probe was placed at the centerline of the exit slot (both in the chordwise and spanwise position, (see figure 19), and the frequency of the actuator was varied within the range of 0 to 300 Hz. Each of these tests was performed at the suction side as well as at the pressure side, which totals to eight test cases.

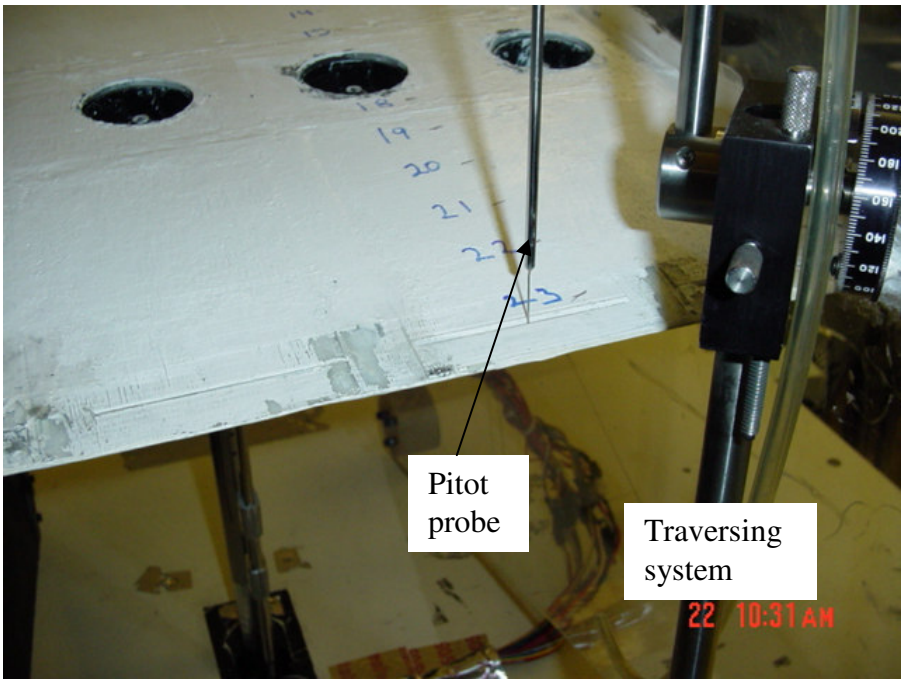

Figure 19: Trailing edge survey using a Pitot tube.

Wind Tunnel Tests

In order to demonstrate the ability to control separation and enhance aerodynamic characteristics of the proposed actuators, the model was tested in the 3'x 4' wind tunnel at the Department of Aerospace Engineering of Texas A&M University. These tests can be divided into the following categories:

Force Balance Tests

These tests were performed for the basic wing with no actuation, for the leading edge actuators with frequency varying from 20 Hz to 60 Hz, with trailing edge actuators for

frequency varying between 100 Hz to 300 Hz at an interval of 100 Hz and with the combination of leading and trailing edge actuators. These tests consisted of pitching the model through a set angle of attack range from -1 to 24 degrees. Data was typically recorded at 2 degree intervals. In the vicinity of the maximum lift coefficient smaller α increments were used where necessary. Pitching moment was taken about 25% of the wing's chord. Data was taken both with and without SJA actuation. The data taken with the actuator off provided a baseline for comparison. In this study, solid and wake blockage were corrected for, using the method presented in Rae and Pope[20].

Flow Visualization Tests

An on-surface flow visualization technique was used. The on-surface visualization used black tufts, placed on the suction side of the wing in order to provide a means of surface flow visualization. All of the above mentioned tests were run in the 3' x 4' tunnel at a free stream velocity of 18 m/s ($Re = 7.1 \times 10^5$) at angles of attack (α) of 20 degrees. All of the flow visualization tests were performed with and without operation of the leading edge actuator only, trailing edge actuator only and a combination of leading and trailing edge actuators. For the case in which the actuators were used, the leading edge actuator was operated at a frequency of 40 Hz and the trailing edge actuator was operated at a frequency of 300 Hz. Video footage and digital still images were recorded during these tests and analyzed subsequently to determine the characteristics of the flowfield for the above-mentioned conditions.

RESULTS AND DISCUSSION

General

The data is presented in the following way:

- Leading edge and trailing edge actuator surveys: Data used to characterize the flowfield at the exit of the SJA slot and that of the trailing edge slot is shown.
- Force Balance Results: Data is presented showing the effect of the synthetic jet actuator on lift, drag and pitching moment.
- On-Surface Flow Visualization: Tufts are also used to provide a second means of surface flow visualization. CFD simulations have also been used to give some insight for understanding the physics involved.

Jet Surveys

This section describes the experiments performed to quantify jet momentum against actuator frequency for the leading as well as the trailing edge actuator

Synthetic Jet Characterization

Figure 20 presents the maximum velocity magnitude, measured at the exit of one of the outer and inner leading edge actuator exit slots in the middle of its width, as a function of actuator frequency. A study is performed to determine compressibility effects. We

define a parameter β to be the ratio of density of air at the exit to its density adjacent to the piston. From continuity arguments it can be shown that

$\beta = k/k_{th}$; $k = S_w V_{\max} / 2\pi f$ and $k_{th} = V_{cyl} / l$

where $V_{\max}$ is the maximum velocity measured at the slot exit, S_w is the slot width, V_{cyl} is the volume of cylinder, f is the frequency of actuation and l is slot length. Figure 20 shows the influence of back compressibility effects. Since the outer slots are wider, flow there is more compressible than that in inner slots.

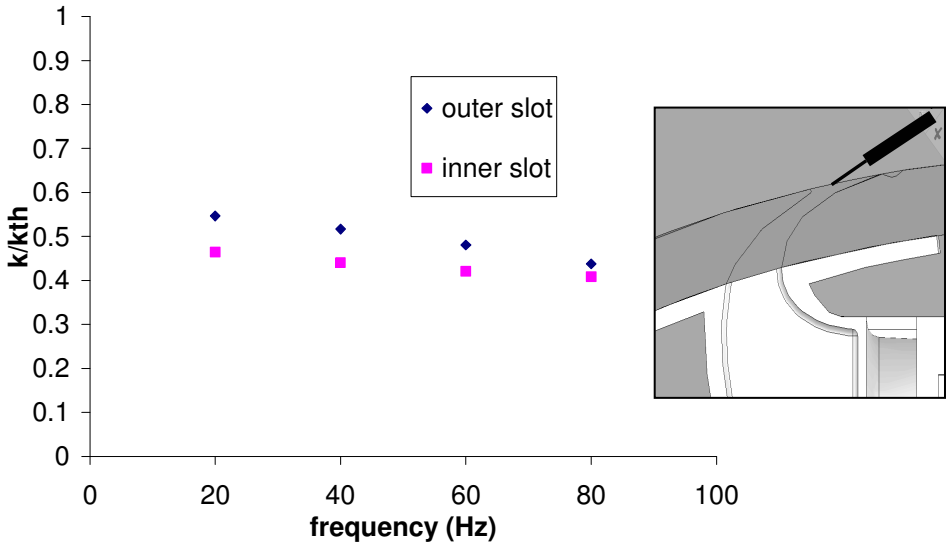

Figure 20: Back compressibility effect at the exit of SJA slots. Actual velocity has been measured using hot wire anemometry.

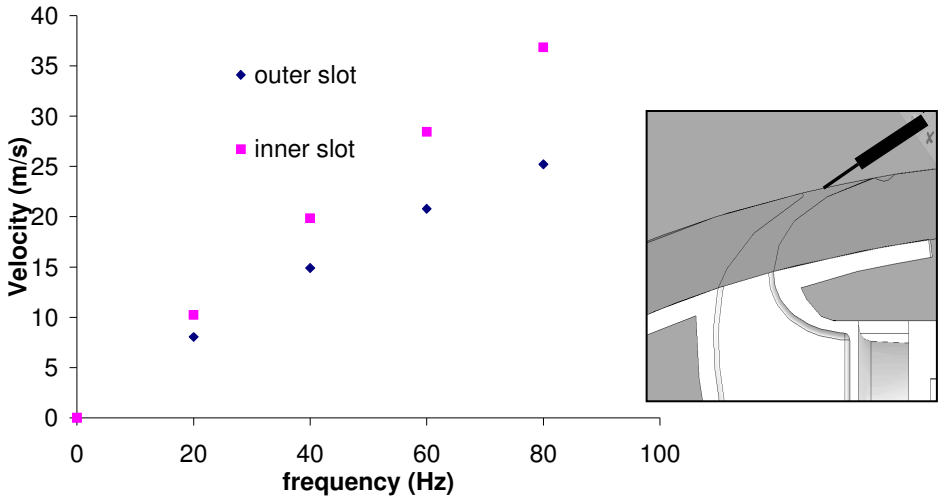

Figure 21: Maximum slot exit velocity as a function of actuator frequency for outer and inner slots.

Table 1 shows the shows the jet momentum coefficient (Cμ) as a function of actuator frequency for each one of the pistons. These values were calculated using the maximum exit velocity of the slot measured experimentally and shown in figures 21 and 22. Consequently the jet momentum coefficient and the actuator frequency may not be varied independently. This is a drawback of the developed system, which is associated with the use of pistons with a fixed stroke length. Some new designs are under development which aims to decouple the frequency with jet momentum. Table 1 shows the variation of area averaged jet momentum coefficient and Strouhal number. As can be seen from Lorber et al.[21], our jet momentum coefficient stays within the effective range.

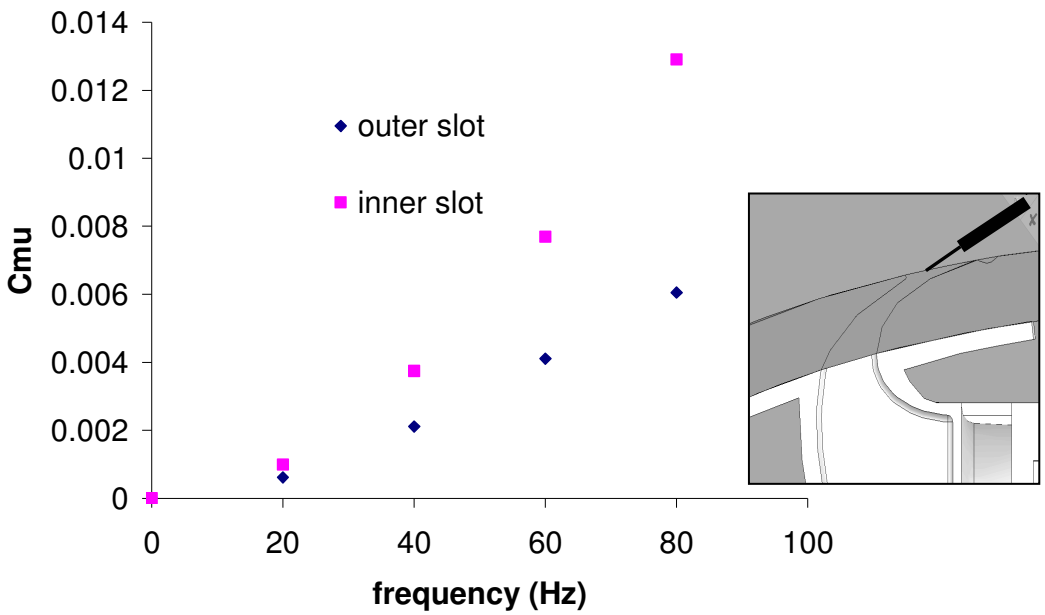

Figure 22: Variation of jet momentum coefficient versus actuator frequency for both inner and outer slots. Comparison based on hot wire data shown in figure 21.

Table 1: Jet momentum coefficient and non dimensional frequency for leading edge actuator frequencies

Frequency of actuator (Hz)	Jet Momentum coefficient, Cμ	Non Dimensional Frequency, F^+
0	0	0
20	0.00068	0.58
40	0.0024	1.17
60	0.0048	1.75
80	0.0074	2.33

Characterization of Trailing Edge Actuator

Velocities at the exit of the trailing edge slots with the jet ejected from the lower surface are measured by using a Pitot tube. The results are shown in figure 23. Measurements are made at the center of each slot in the chordwise and spanwise directions and we assume uniform velocity profile through each slot for calculating the jet momentum coefficient associated with trailing edge actuator. The internal flap rests against the upper wall forcing the jet out of the lower surface. Similarly figure 24 shows the air velocity measured against fan frequency for the jet ejected from the upper surface.

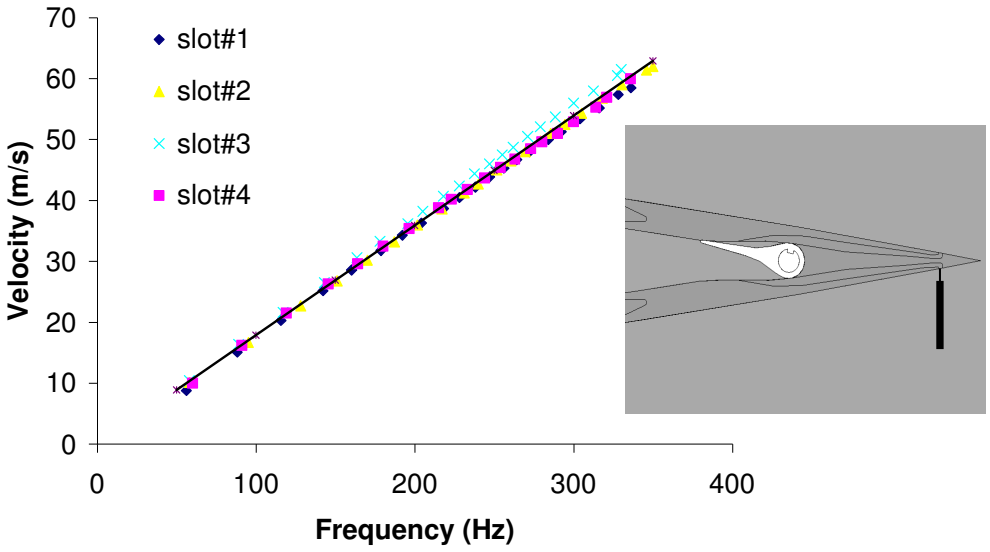

Figure 23: Variation of air velocity with fan frequency at the exit of all slots when jet is ejected from the lower surface. Solid line marks average velocity over the slots against average fan frequency.

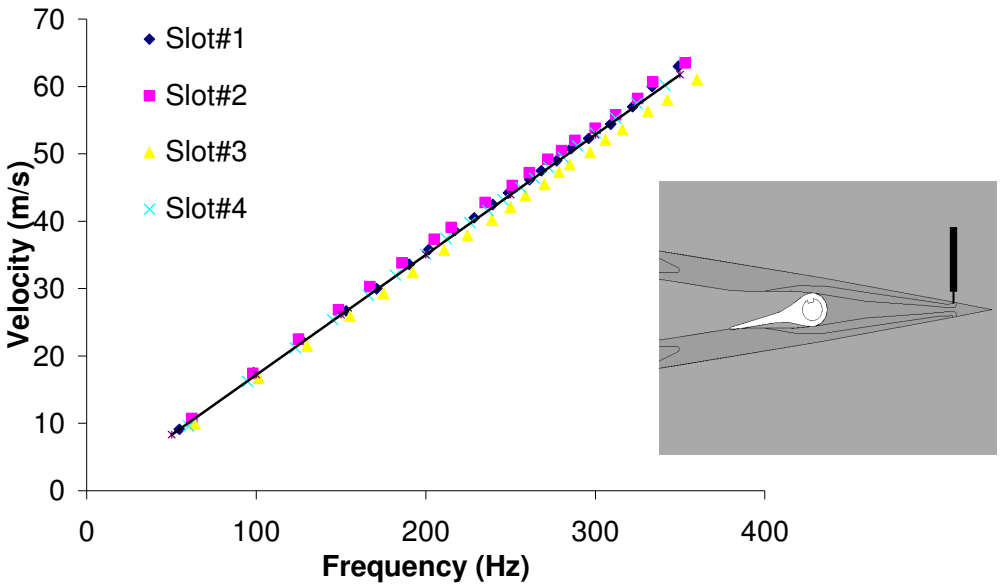

Figure 24: Variation of air velocity with fan frequency at the exit of all slots when jet is ejected from the upper surface. Solid line marks average velocity over the slots against average fan frequency.

Figure 25 shows the variation of the jet momentum coefficient against fan frequency. As it is clearly visible, the momentum coefficient for the lower surface is slightly different from that of the upper surface. This difference may be because of asymmetry caused by the configuration of fans and that induced by errors in manufacturing through Rapid Prototyping.

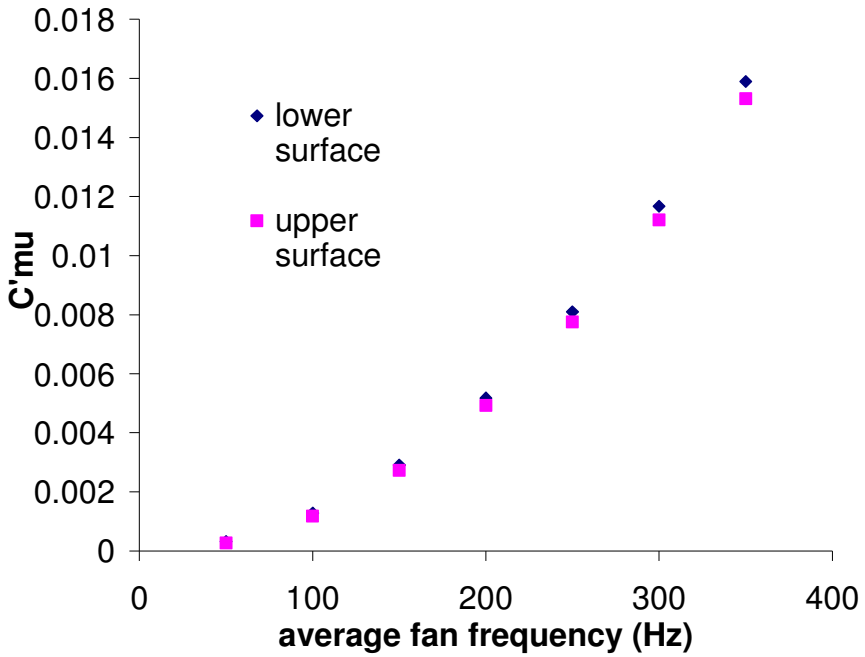

Figure 25: Variation of average jet momentum coefficient C'_{μ} with average fan frequency.

Force Balance Results

Force balance tests were performed for 3 cases which included

a) Effect of leading edge actuation on lift, drag and pitching moment.

b) Effect of trailing edge actuation on lift, drag and pitching moment.

c) Influence of combined actuation (leading and trailing edge) on lift, drag and pitching moment.

Effect of Leading Edge Actuation on Aerodynamic Properties

Figure 26 shows the effect of synthetic jet actuation on the lift coefficient. As it is clearly visible, leading jet actuation has a predominant effect on the delay of stall, which leads to increase of the maximum lift coefficient CL_{max}. Another observation is regarding the type of stall that occurs with synthetic jet actuation. The baseline shows a very docile stall, typical of thick airfoils, which is also known as trailing edge stall. With SJA there is a sharp decrease in lift coefficient after it attains its peak. This should be the case as at stall angles the adverse pressure gradient is too severe to be controlled by SJA, and once flow separates, SJA has little role in attaching it even partially, causing there to be a massive separation.

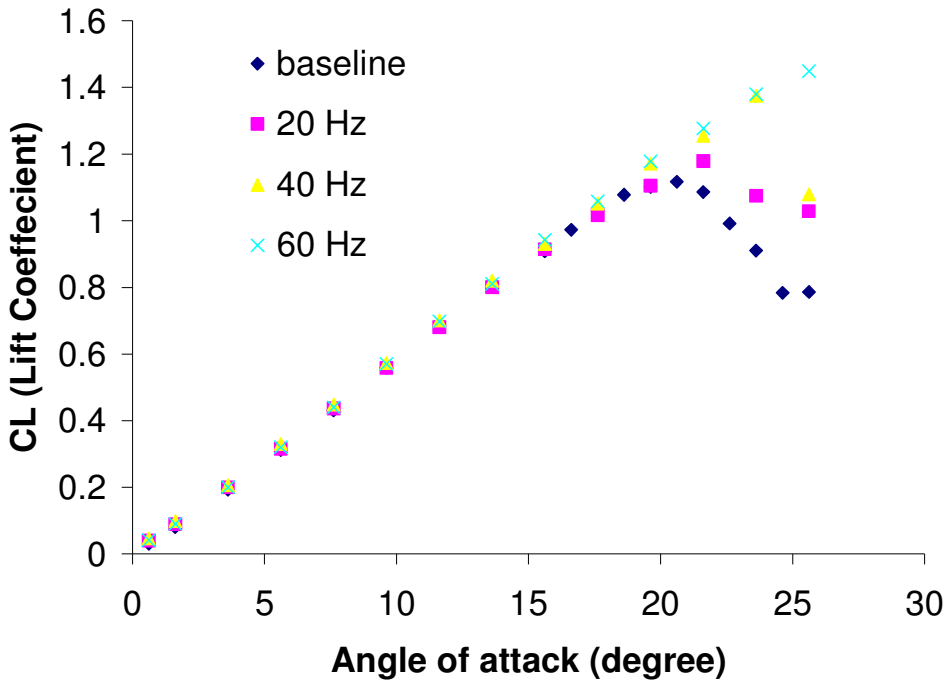

Figure 26: Effect of synthetic jet actuator on aerodynamic performance of test wing. Lift coefficient (CL) vs. angle of attack.

Another important observation is that SJA cannot improve lift coefficient at low angle of attacks, a feature that is central cause of the present study. Figure 27 shows that variation of drag coefficient CD versus lift coefficient CL and figure 28 shows the variation of pitching moment coefficient Cm versus lift coefficient CL.

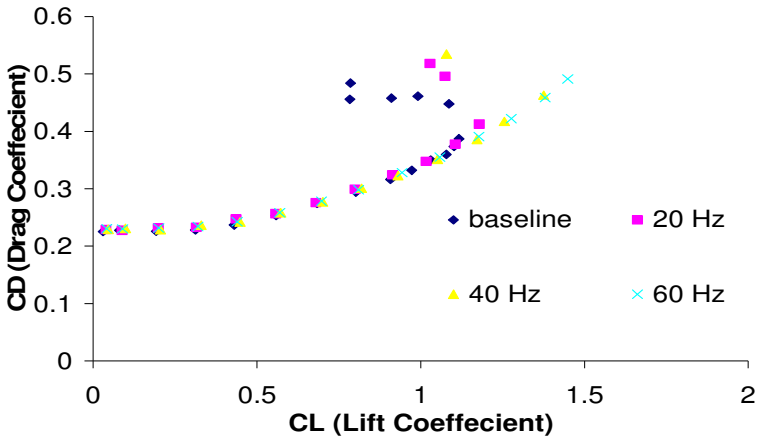

Figure 27: Effect of synthetic jet actuator on aerodynamic performance of test wing. Drag coefficient (CD) vs. lift coefficient (CL).

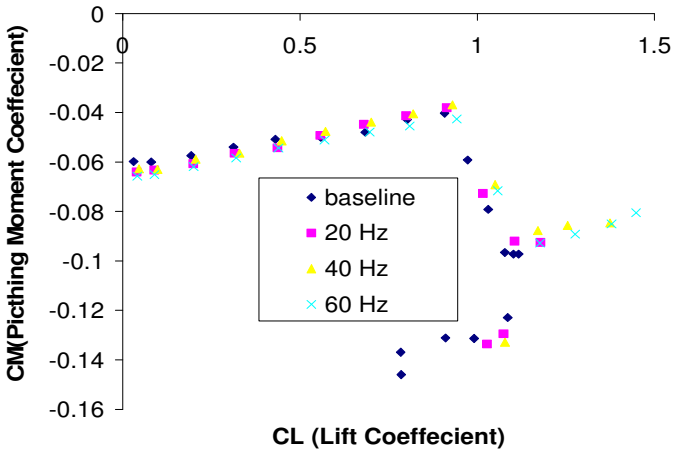

Figure 28: Effect of synthetic jet actuator on aerodynamic performance of test wing. Pitching moment coefficient (Cm) vs. lift coefficient (CL).

It is clearly visible that SJA has profound effects in increasing stall angle and hence keeping flow attached at higher angles, but in all figures (26 through 28) we can observe hardly any influence of actuation in the pre stall regime, which is the central cause of the present study.

Effect of Trailing Edge Actuation on Aerodynamic Properties

In this section we present force balance results on the effects of trailing edge actuation alone. The angle of attack is again varied from -1^o to 24^o, with 2^o increments, with more resolution where required. Smaller The fan frequencies used were 100, 200 and 300 Hz. Data is presented for jet ejecting from the lower surface (internal flap resting against top wall) as well as for jet ejecting from the upper surface.

Jet Ejecting from Lower Surface

Figures 29 through 31 show the effect of the trailing edge actuator with the jet ejecting from the lower surface. As it is visible from figure 29, there is lift enhancement even at low angles of attack. This is due to the jet flap effect. As angle of attack increases, the slope of the lift curve is increased. The fact that there is appreciable change in the jet angle with respect to free stream, causing a higher pressure difference at the jet, may attribute towards this increase. At higher angles, where separation starts, the fans installed at the suction side suck in the low momentum air and delay separation.

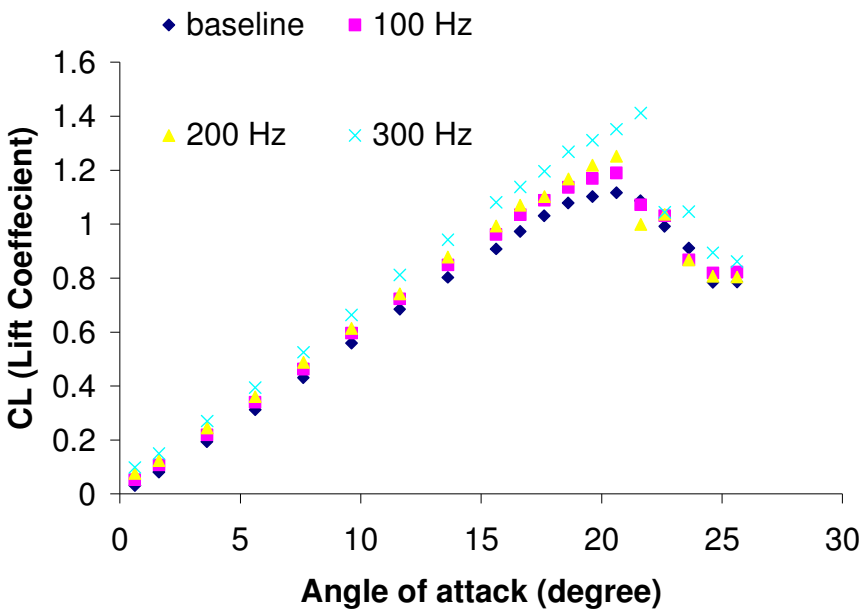

Figure 29: Effect of trailing edge actuator with jet ejecting from lower surface on aerodynamic performance of test wing. Lift coefficient (CL) vs. angle of attack.

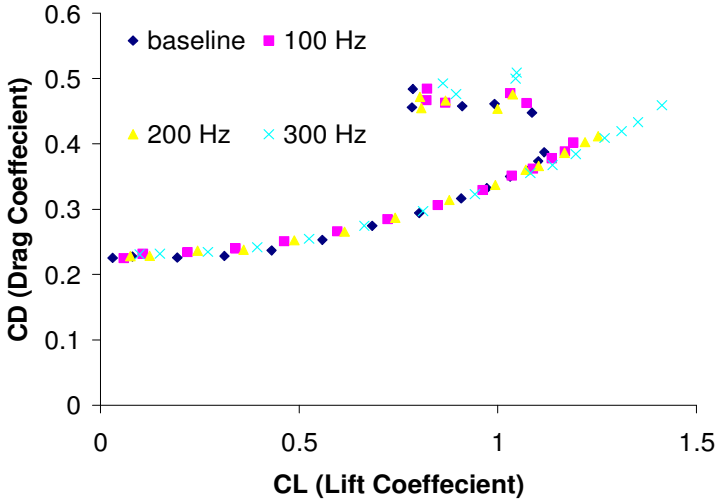

Figure 30: Effect of trailing edge actuator with jet ejecting from lower surface aerodynamic performance of test wing. Drag coefficient (CD) vs. lift coefficient (CL).

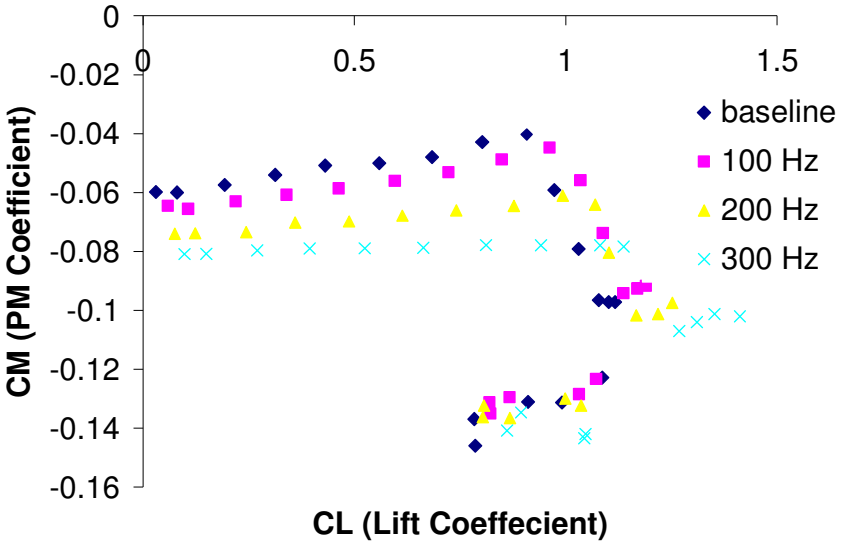

Figure 31: Effect of trailing edge actuator with jet ejecting from lower surface on aerodynamic performance of test wing. Pitching moment coefficient (Cm) vs. lift coefficient (CL).

Figure 30 shows the effect on drag coefficient. At low angles, it should be guessed that the propulsive forces generated would reduce drag and therefore the curve seems baffling initially. The explanation comes from the fact that we are using very low values of jet momentum coefficient which exerts negligibly small thrusts. We even ran some tests without any flow to measure the effect of propulsive thrust on lift force, but the forces were so small that the balance used could not detect it. Further, the ejection of jet is not exactly at the trailing edge. This causes some separation between the jet and the sharp trailing edge. The two effects stated cumulatively explain the fact that there is no effect of actuation on drag coefficient (CD) at low angles of attack. At high angles, there is attachment due to boundary layer control by the fans. Figure 31 shows the effect of

trailing edge actuation in the current mode of the internal flap, on pitching moment coefficient (Cm). As can be seen, there is a huge increment (almost 50%) in the nose down moment. This is because the rear of the airfoil gets loaded more due to the jet flap effect. Again the suction effect is visible at higher lift coefficients.

Effect of Trailing Edge Actuation with Jet Ejecting from Upper Surface

Figures 32 through 34 show the effect of trailing edge actuation with jet ejecting from the upper surface (internal flap resting against bottom wall) on aerodynamic properties. As can be seen from figure 32, the lift coefficient becomes negative at low incidence, intersects the baseline curve and goes through a peak before stalling. Again, the former effect can be attributed to the jet flap effect, although used in an unconventional way. It is visible that the slope of the lift curve increases even at low angles of attack, an observation that is due to the change in jet flap angle with angle of attack. It is seen that the actuated curves intersect the baseline at an angle of attack of 16^{o}, an angle where separation starts commencing for the baseline. Clearly, boundary layer control due to suction dominates at this point. Figure 33 shows the effect of the actuation on drag coefficient (CD), here we observe an increase in drag coefficient at low angles. The effect of jet flap and separation at the trailing edge, as explained in the previous section, explain the trend. Boundary layer control is also clearly visible at higher angles of attack. Figure 34 shows the effect on pitching moment coefficient (Cm). Here there is no clear trend visible, except for the boundary layer control at higher lift coefficients.

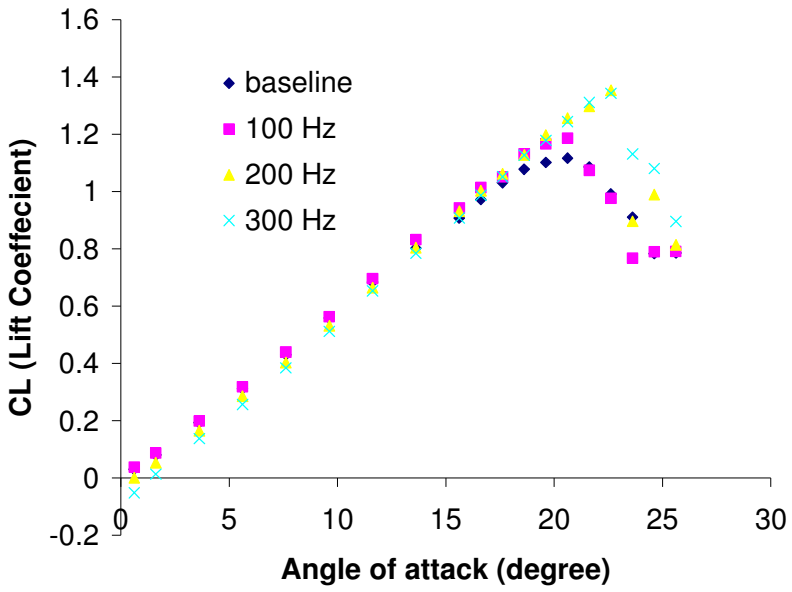

Figure 32: Effect of trailing edge actuator with jet ejecting from upper surface on aerodynamic performance of test wing. Lift coefficient (CL) vs. angle of attack.

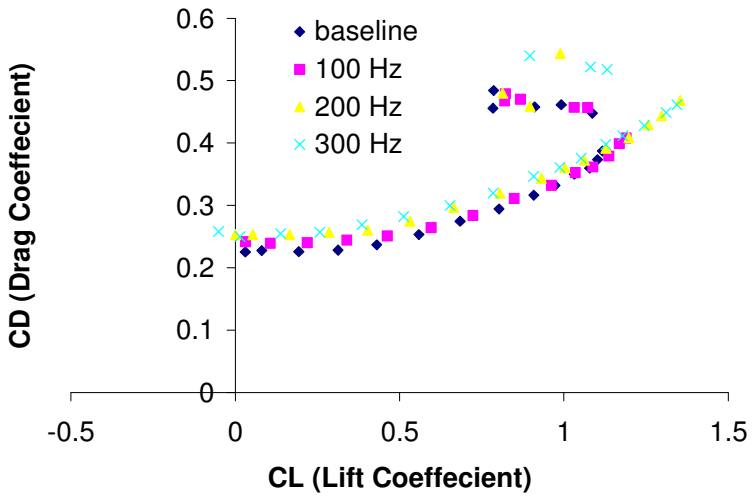

Figure 33: Effect of trailing edge actuator with jet ejecting from upper surface on aerodynamic performance of test wing. Drag coefficient (CD) vs. lift coefficient (CL).

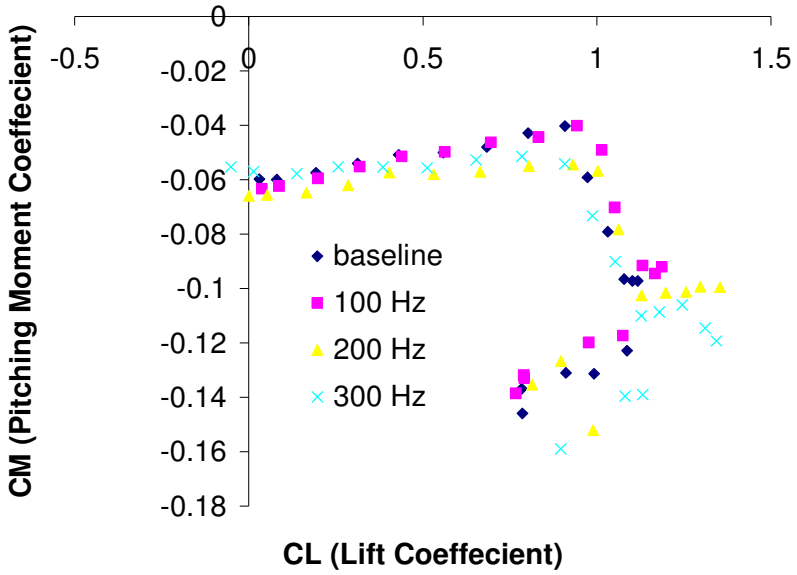

Figure 34: Effect of trailing edge actuator with jet ejecting from upper surface on aerodynamic performance of test wing. Pitching moment coefficient (Cm) vs. lift coefficient (CL).

More investigation with higher jet momentum coefficient may shed some light on the missing trends at low values of the lift coefficient (CL).

Combined Effects of Leading Edge Actuation and Trailing Edge Actuation

In this section we present force balance results for the combined effects of the SJA and the trailing edge actuation. The angle of attack is typically varied from -1^{o} to 24^{o}, with 2^{o} increments. Smaller increments have been used whenever necessary. Fan frequency used was 300 Hz. SJA frequency was varied from 0 to 40 Hz for the case when the jet is

ejected from the upper surface and from 0 to 60 Hz when the jet is ejected from the lower surface.

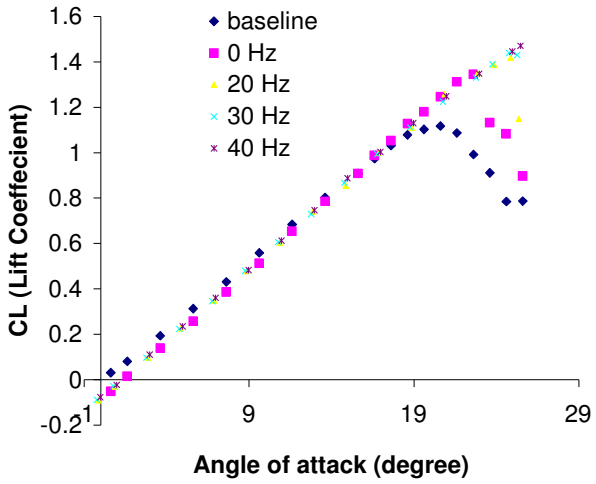

Figure 35: Effect of variation in leading edge actuator frequency and trailing edge actuator at 300 Hz with jet ejecting from upper surface on aerodynamic performance of test wing. Lift coefficient (CL) vs. angle of attack.

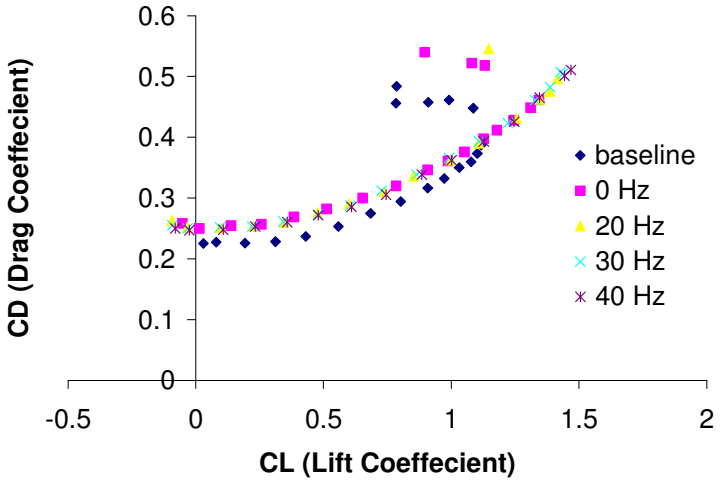

Figure 36: Effect of variation in leading edge actuator frequency and trailing edge actuator at 300 Hz with jet ejecting from upper surface on aerodynamic performance of test wing. Drag coefficient (CD) vs. lift coefficient (CL).

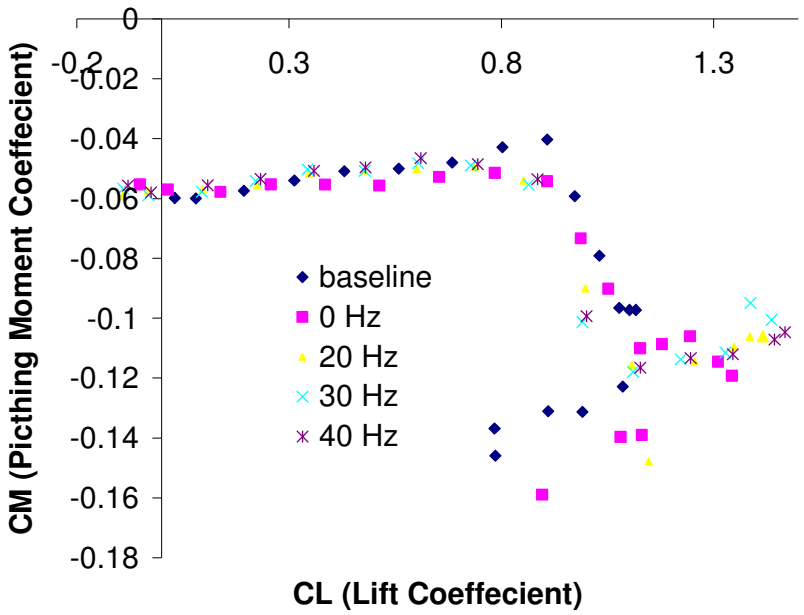

Figure 37: Effect of variation in leading edge actuator frequency and trailing edge actuator at 300 Hz with jet ejecting from upper surface on aerodynamic performance of test wing. Pitching moment coefficient (Cm) vs. lift coefficient (CL).

Jet Ejecting from Upper Surface

Figures 35 through 37 present the data for this section. It can be observed that for all cases, SJA did not have any effect on aerodynamic properties at low incidence, albeit, at high incidence SJA is very effective in containing separation. We will discuss more about an important feature of this flow control configuration in the next section.

Jet Ejecting from Lower Surface

Figures 38 through 40 show the effects of SJA on the wing controlled by the trailing edge actuation at 300 Hz. This data again shows the minimal effect of SJA on

aerodynamic properties at low incidence. At high incidence SJA does delay separation as is visible from the increase in stall angle of attack and maximum lift coefficient (CL), but the effect, even at 60 Hz of SJA frequency, is not as much as that for the case when the jet ejects from the upper surface in the previous section. The reason for this difference in behavior is that when the jet ejects from the upper surface, the wing is less loaded and the pressure on the suction side is higher near the trailing edge, causing the adverse pressure gradient to be lower; thus, even after flow separation, the SJA controls separation effectively due to comparatively lower adverse pressure gradient than for the present case. For the present case the pressure gradient is steeper and the SJA is therefore less effective in attaching the flow at higher angles of attack due to more aerodynamic loading.

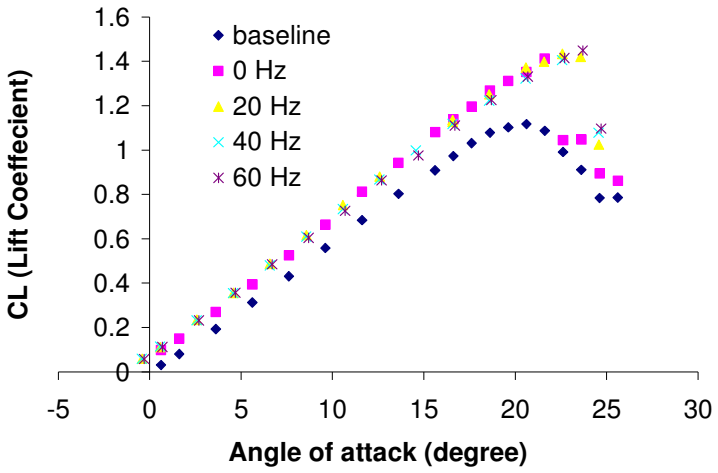

Figure 38: Effect of variation in leading edge actuator frequency and trailing edge actuator at 300 Hz with jet ejecting from lower surface on aerodynamic performance of test wing. Lift coefficient (CL) vs. angle of attack.

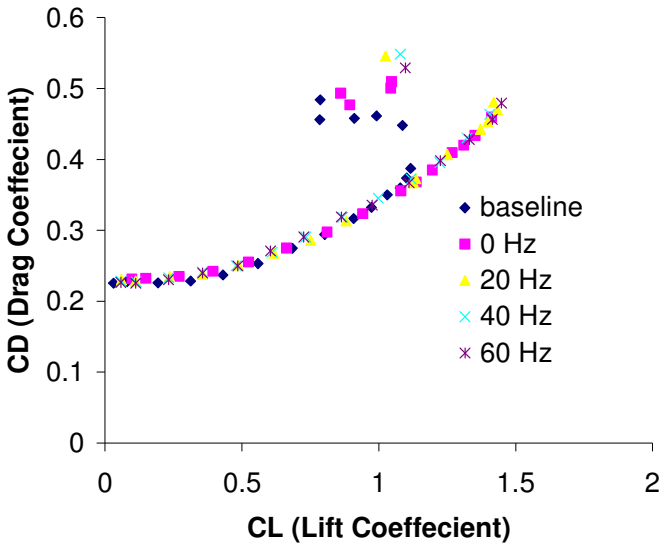

Figure 39: Effect of variation in leading edge actuator frequency and trailing edge actuator at 300 Hz with jet ejecting from lower surface on aerodynamic performance of test wing. Drag coefficient (CD) vs. lift coefficient (CL).

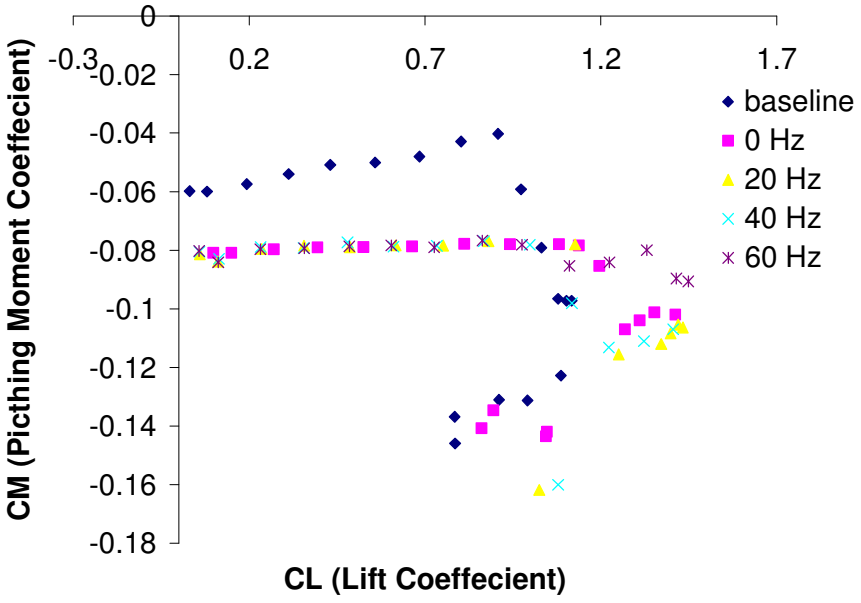

Figure 40: Effect of variation in leading edge actuator frequency and trailing edge actuator at 300 Hz with jet ejecting from lower surface on aerodynamic performance of test wing. Pitching moment coefficient (Cm) vs. lift coefficient (CL).

Flow Visualization Results

Figures 41 through 45 show the results obtained by the use of tufts as a surface visualization device. The use of tufts permitted the observation of the flowfield characteristics in “real-time”, and the effects of having or not having SJA control on the wing were clearly visible without having to change the operating conditions of the wind tunnel as in the case of oil surface flow visualization.

For these tests, the freestream velocity (U_∞) had a value of 18 m/s. Data was taken at angles of attack of 20 degrees. Figure 42 shows the basic wing with no actuation. It can be seen that the tufts move away from surface close to the leading edge at around 20% of the chord. This marks the separation point. Figure 42 shows the effect when the trailing edge actuator with the jet ejecting from the lower surface is engaged at a frequency of 300 Hz. The flow attaches up to around 55 % of chord length. Figure 43 shows that the flow gets attached over the entire length of airfoil as soon as SJA is engaged at 40 Hz along with the trailing edge actuation as in the previous case. Figure 44 and figure 45 show the same effect for the case when the jet ejects from the upper surface. Similar observations can be made.

Figure 41: Tufts flow visualization of test wing. No control.

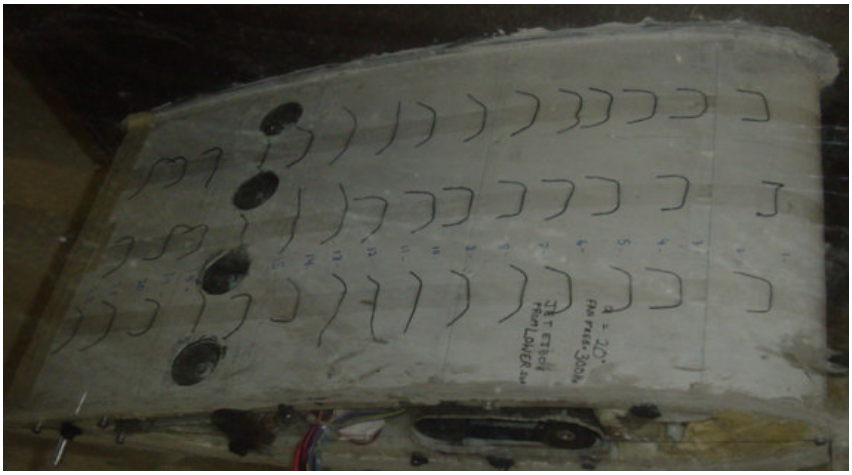

Figure 42: Tufts flow visualization of test wing. Trailing edge actuator control with jet ejecting from lower surface at 300 Hz.

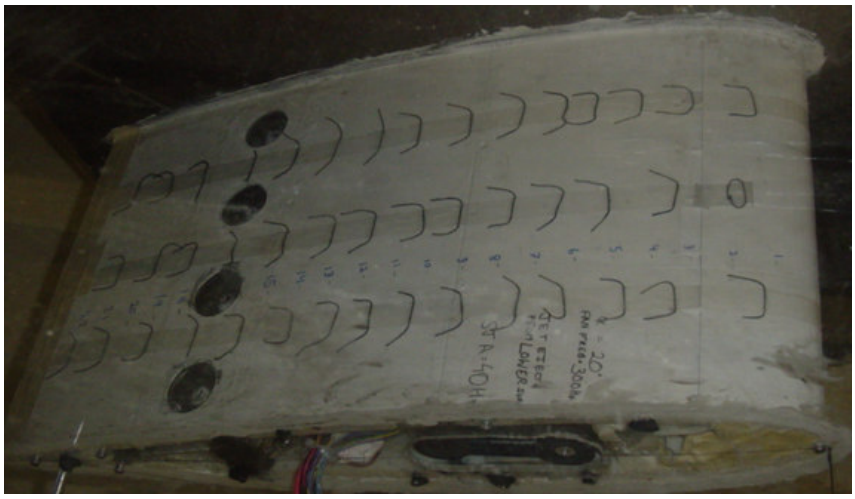

Figure 43: Tufts flow visualization of test wing. Trailing edge actuator control with jet ejecting from lower surface at 300 Hz and SJA control at 40 Hz.

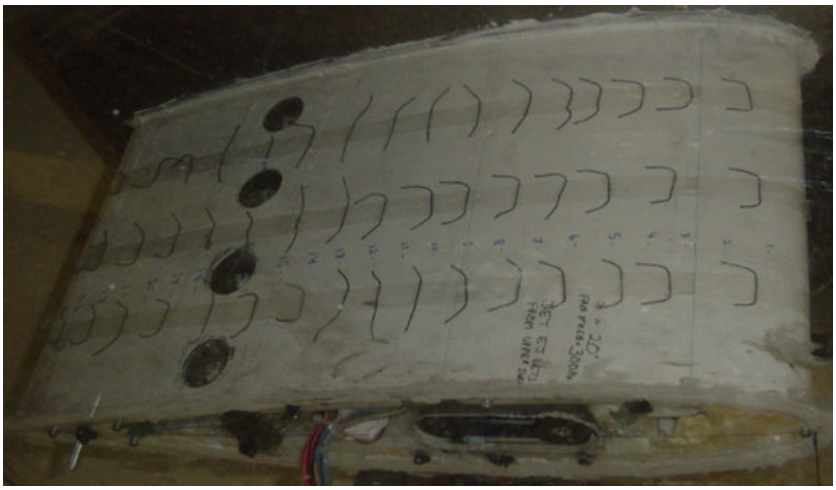

Figure 44: Tufts flow visualization of test wing. Trailing edge actuator control with jet ejecting from upper surface at 300 Hz.

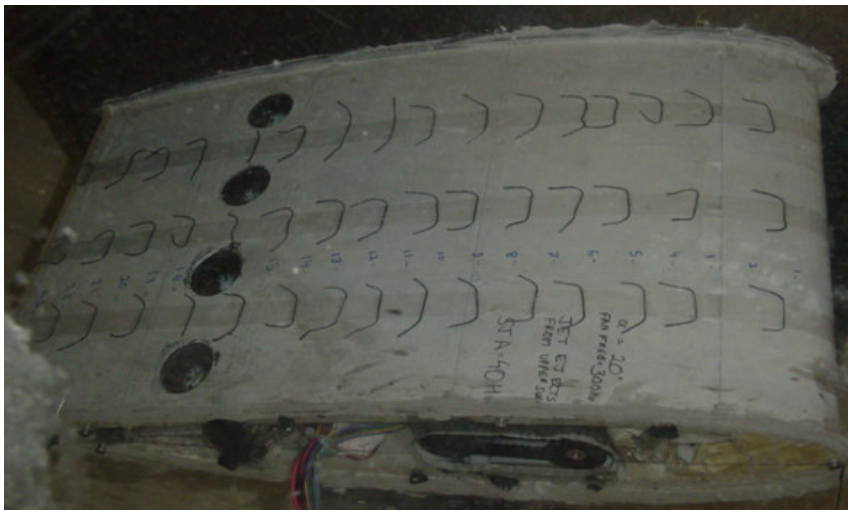

Figure 45: Tufts flow visualization of test wing. Trailing edge actuator control with jet ejecting from upper surface at 300 Hz and SJA control at 40 Hz.

CONCLUSIONS AND RECOMMENDATIONS

This research presents the development of a trailing edge actuator intended to harness the potential of boundary layer control and the jet flap effect in an innovative manner. The study evaluates the effect of leading jet actuation in conjunction with the effect of trailing edge actuation on the flowfield.

An initial survey using hot wires for the leading edge actuator showed a maximum velocity of around 38 m/s for a frequency of 80 Hz. A Pitot tube survey of the trailing edge actuator showed the maximum velocity at 350 Hz can be up to 62 m/s. More sophisticated design of trailing edge ducts and higher fan frequency will result in higher velocity. An advantage of this type of actuator was the decoupling of the jet flap from the aircraft engine, which in case of asymmetric engine failure, can lead to catastrophic imbalance in roll moments. The developed actuators are put inside a NACA 0015 airfoil with a chord length of 0.6 m and span of 0.32 m.

The actuators were placed in a NACA 0015 wing that was tested in a wind tunnel. An experimental investigation into the effects of the synthetic jet actuator, the trailing edge actuator and their combined effect on the performance of the wing was described. Emphasis was placed on the capabilities of the actuator to control the separation of the flow over the wing at high angles of attack. The limitation of the synthetic jet actuator

was addressed using advantages of the trailing edge actuator by implementing both the actuators in tandem. The investigation included the use of force balance measurements and on-surface flow visualization with tufts. All the tests were performed at a freestream velocity of 18 m/s, corresponding to a Reynolds number of 7.1 $x10^5$. The angle of attack (α) was varied from –1 to 24 degrees.

For the tests presented here, at $\alpha < 16$ degrees, the leading edge actuator provides no perceptible control. At higher angles of attack, the SJA extends the range of α for which the wing may be operated without stalling. The use of SJA increased the stall angle to 24 degrees, the maximum angle attainable, and a corresponding increase in CL_{max} of around 30% occured. The trailing edge actuator was tested in both configurations – with the jet ejecting from the upper surface and ejecting from the lower surface. Both configurations provided low angle control; lift at low incidence angle decreased for the former case and increased for the latter case. Such an arrangement provides a way to control rolling motion of an aircraft without any mechanical flap. At higher angles, boundary layer suction was predominant as suggested by the force balance experiments. Combined tests showed that SJA was effective in controlling separation, but its effect was higher in the case where the jet ejects from the upper surface. This is due to less aerodynamic loading.

On-surface flow visualization was performed at the suction side of airfoil, and still photographs show the effect of boundary layer control and synthetic jet actuation. More study is needed to optimize the design of the leading and trailing edge actuators and to

model the effect of these phenomena. Future work should concentrate on methodologies of using higher momentum coefficients by increasing fan frequency and optimizing slot design. Efforts are underway to decouple SJA frequency from its jet momentum coefficient, which would provide far more flexibility in hingeless flow control.

REFERENCES

[1]Klausmeyer, S. M., Papadakis, M., and Lin, J. C., "A Flow Physics Study of Vortex Generators on a Multi- Element Airfoil," AIAA Paper 96-0548, 34th Aerospace Sciences Meeting and Exhibit, Reno, NV, 1996.

[2]Chang, R. C., Hsiao, F. B., and Shyu, R. N., "Forcing Level Effects of Internal Acoustic Excitation on the Improvement of Airfoil Performance," *Journal of Aircraft*, Vol. 29, No. 5, 1992, pp. 823-829.

[3]Huang, R. F., and Mao, S. W., "Separation Control on a Cantilever Wing with a Self-Excited Vibrating Rod," *Journal of Aircraft*, Vol. 39, No. 4, 2002, pp. 609-615.

[4]Kruger, W., "Drag Reduction by Suction of the Boundary Layer Separated Behind Shock Wave Formation at High Mach Numbers," *NACA Technical Memorandum* No. 1168, Washington, 1947.

[5]Goodmanson, L. T., and Gratzer, L. B., "Recent Advances in Aerodynamics for Transport Aircraft – Part 1", *Astronautics and Aeronautics*, Vol. 11, 1973, pp. 30-45.

[6]Goodmanson, L. T., and Gratzer, L. B., "Recent Advances in Aerodynamics for Transport Aircraft – Part 2", *Astronautics and. Aeronautics*, Vol. 12, 1974, pp. 52-60.

[7]Tillman, T. G. and Hwang, D. P., "Drag Reduction on a Large-Scale Nacelle Using a Micro-Blowing Technique," AIAA 99-0130, 37th Aerospace Sciences Meeting & Exhibit, Reno, NV, 1999.

[8]Gad-el-Hak, M., *Flow Control: Passive, Active, and Reactive Flow Management*, Cambridge University Press, New York, 2000, pp. 150-188.

[9]Seifert, A., and Pack, L., "Dynamics of Active Separation Control at High Reynolds Numbers," AIAA Paper No. 2000-0409, 38th Aerospace Sciences Meeting and Exhibit, Reno, NV, 2000.

[10]Seifert A., Bachat T., Koss D., Shepshelovich M., Wygnanski I., "Oscillatory Blowing: A Tool to Delay Boundary-Layer Separation", AIAA *Journal*, Vol. 31, 1993, pp. 2052-2060.

[11]Rathnasingham, R. and Breuer, K., "Coupled Fluid-Structural Characteristics of Actuators for Flow Control," *AIAA Journal*, Vol. 35, 1997, pp. 832-837.

[12] Seifert, A, Eliahu, S, Greenblatt, D, Wygnanski, I., "On the Use of Piezoelectric Actuators for Airfoil Separation Control," *AIAA Journal*, Vol. 36, 1998, pp.1535-1537.

[13]Seifert, A., and Pack, L., "Oscillatory Control of Separation at High Reynolds Numbers," *AIAA Journal*, Vol. 37, 1999, 1062-1071.

[14]McCormick, D., "Boundary Layer Separation Control with Directed Synthetic Jets," AIAA Paper 2000-0519, 38th Aerospace Sciences Meeting and Exhibit, Reno, NV, 2000.

[15]Greenblatt, D., and Wygnanski, I., "Dynamic Stall Control by Periodic Excitation, Part 1: NACA 0015 Parametric Study", *Journal of Aircraft*, Vol. 38, No. 3, 2001, pp. 430-438.

[16]Gilarranz, J. L. and Rediniotis, O. K., "Compact, High-Power Synthetic Jet Actuators for Flow Separation Control," AIAA Paper 2001-0737, 39th Aerospace Sciences Meeting and Exhibit, Reno, NV, 2001.

[17]Gilarranz , J. L., Traub, L. W., and Rediniotis, O. K., "Characterization of a Compact, High-Power Synthetic Jet Actuator for Flow Separation Control," AIAA Paper 2002-0127, 40th Aerospace Sciences Meeting and Exhibit, Reno, NV, 2002.

[18]Davidson I. M., "The Jet Flap," *J. Royal Aeronautical Soc.* Vol. 60, 1956, pp. 25 - 50.

[19]Williams J., Butler, S. F. J., and Wood M. N., "The Aerodynamics of Jet Flaps," *Aeronautical Research Council, Reports and Memoranda,* No. 3304, Bedford, Great Britain, 1963.

[20]Rae, W., and Pope, A., *Low-speed Wind Tunnel Testing*, John Wiley and Sons, New York, 1984, pp. 344-401.

[21]Lorber, P., McCormick, D., Anderson, T., Wake, and MacMartin, B., "Rotorcraft Retreating Blade Stall Control," AIAA Paper 2000-2475, 38th Aerospace Sciences Meeting and Exhibit, Reno, NV, 2000.

APPENDIX

Definition of Non Dimensional Coefficients Used

Reynolds number, $\mathrm{Re} = \dfrac{\rho U_{\infty} c}{\nu}$

Lift coefficient, $CL = \dfrac{L}{\frac{1}{2}\rho U_{\infty}^{2} cs}$

Drag coefficient, $CD = \dfrac{D}{\frac{1}{2}\rho U_{\infty}^{2} cs}$

Pitching moment coefficient, $Cm = \dfrac{PM}{\frac{1}{2}\rho U_{\infty}^{2} c^{2} s}$

Non dimensional frequency, $F^{+} = \dfrac{f x_{te}}{U_{\infty}}$

Jet momentum coefficient for trailing edge actuator, $C'\mu = \dfrac{\rho U^{2} l \delta}{\frac{1}{2}\rho U_{\infty}^{2} cs}$

where *l* is the total length of slots in spanwise direction and δ is slot width, U is the exit air velocity at the slot.

Jet momentum coefficient for leading edge actuator, $C\mu = \frac{\rho U^2 l S_w}{\frac{1}{2}\rho U_\infty^2 cs}$

where *l* is the total length of slots in spanwise direction and S_w is slot width, U is the maximum exit air velocity at the slot.

Other symbols have usual meanings.

VITA

Name:		Anmol Agrawal
Email:		anmol.aggie@gmail.com
Address:		Department of Mechanical Engineering Texas A&M University Mail Stop 3123 College Station, Texas 77843-3123
Education:		M.S., Mechanical Engineering (December 2005) Texas A&M University B.E., Mechanical Engineering (June 2002) Motilal Nehru National Institute of Technology Allahabad, India
Work Experience:	09/04-12/05	Graduate Research Assistant Fluid Dynamics Laboratory Aerospace Engineering Department Texas A&M University
	09/03-08/04	Teaching Assistant Numerical Analysis for Mechanical Engineers (MEEN-361) Mechanical Engineering Department Texas A&M University
	07/02-08/03	Programmer Analyst Cognizant Technology Solutions Chennai, India